EBioMedicine 45 (2019) 92–107

Contents lists available at ScienceDirect

EBioMedicine

journal homepage: www.ebiomedicine.com

EBioMedicine
Published by THE LANCET

Research paper

A role for kinesin-1 subunits KIF5B/KLC1 in regulating epithelial mesenchymal plasticity in breast tumorigenesis

Alaa Moamer, Ibrahim Y. Hachim, Najat Binothman, Ni Wang, Jean-Jacques Lebrun, Suhad Ali *

Department of Medicine, Cancer Research Program, Centre for Translational Biology, McGill University Health Centre, McGill University, Canada

ARTICLE INFO

Article history:
Received 1 November 2018
Received in revised form 3 June 2019
Accepted 6 June 2019
Available online 14 June 2019

Keywords:
Epithelial mesenchymal plasticity
KIF5B
KLC1
Prolactin
TGFβ
EMT
Invasion
Xenograft
Differentiation
Cancer stem cells

ABSTRACT

Background: Epithelial mesenchymal plasticity (EMP) is deemed vital in breast cancer progression, metastasis, stemness and resistance to therapy. Therefore, characterizing molecular mechanisms contributing to EMP are in need enabling the development of more advanced therapeutics against breast cancer. While kinesin superfamily proteins (KIFs) are well known for their role in intracellular cargo movement, our knowledge of their function in breast tumorigenesis is still limited.

Methods: Various breast cancer cell lines representing different molecular subtypes were used to determine the role of kinesine-1 subunits KIF5B/KLC1 in regulation of EMP.

Findings: In breast cancer, we show that kinesin family member 5B (KIF5B) and its partner protein kinesin light chain 1 (KLC1), subunits of kinesin-1, to play differential roles in regulating EMP and tumorigenesis. Indeed, we found KIF5B to be expressed in triple negative (TN)-basal-like/claudin low breast cancer subtype and to be an inducer of epithelial-mesenchymal transition (EMT), stemness, invasiveness, tumor formation and metastatic colonization. Whereas, we found KLC1 to be expressed in epithelial/luminal breast cancer subtypes and to be a suppressor of EMT, invasion, metastasis and stem cell markers expression as well as to be an inducer of epithelial/luminal phenotype. Interestingly, in TN-basal-like/claudin low cells we found a novel nuclear accumulation of KIF5B and its interaction with the EMT transcriptional regulator Snail1 independent of KLC1. In addition, TGF-β mediated pro-invasive activity was found to be dependent on KIF5B expression. In contrast, the epithelial differentiation factor and EMT suppressor prolactin (PRL) was found to repress KIF5B gene expression and KIF5B-Snail1 nuclear accumulation, but enhanced KLC1 gene expression and KIF5B-KLC1 interaction.

Interpretation: Together, these results highlight a new paradigm for kinesin-1 function in breast tumorigenesis by regulating EMP programing and aggressiveness.

Fund: This work was supported by the Canadian Institutes of Health Research (operating grants #233437 and 233438) granted to Suhad Ali.

1. Introduction

Despite improvements in early detection and advances in treatment options, breast cancer progression to a metastatic disease remains a major clinical challenge. Epithelial mesenchymal plasticity (EMP) is now well recognized cellular process contributing to cancer cell diversity and intra-tumor heterogeneity associated with disease progression and impaired response to therapy [1,2]. The role of EMP in promoting aggressive breast cancer phenotype is further emphasized in recent molecular subclassification of breast cancer. Indeed the mesenchymal-basal-like (claudin low) TNBC subtype, frequently characterized by high histological grade and poor differentiation, to be associated with unfavorable pathological features and poor patient outcome in comparison to the epithelial/luminal subtypes [3,4]. Furthermore, pro-oncogenic and pro-metastatic growth factors such as TGF-β are known to potently induce EMT and promote the transition of breast cancer cells from non-invasive epithelial to invasive mesenchymal with stem-like phenotype [5,6]. Conversely, EMT suppressors such as prolactin hormone (PRL), is shown to supress the mesenchymal properties and induce an epithelial phenotype in breast cancer cells and subsequently supress their invasive and tumorigenic behaviour [7,8]. Therefore, regulators of EMP represent important targets for the development of novel therapeutics in breast cancer. Clinically, whereas current targeted breast cancer treatments are directed toward the epithelial/luminal subtypes, there are no targeted treatments for the

* Corresponding author at: MUHC-RI, Office E 02.6232, 1001 Decarie Blvd, Montreal, Quebec H4A 3J1, Canada.
E-mail addresses: alaa.moamer@mail.mcgill.ca (A. Moamer), ibrahim.hachim@mail.mcgill.ca (I.Y. Hachim), najat.binothman@mail.mcgill.ca (N. Binothman), ni.wang79@gmail.com (N. Wang), jj.lebrun@mcgill.ca (J.-J. Lebrun), suhad.ali@mcgill.ca (S. Ali).

https://doi.org/10.1016/j.ebiom.2019.06.009

Research in context

Evidence before this study

Kinesin superfamily proteins (KIFs) are well known to be involved in intracellular movement and cytoplasmic transport of membranous organelles and macromolecules including complex proteins as well as RNA along the microtubules network. Kinesin-driven transport along microtubules is mediated by the concerted function of two kinesin subunits, the kinesin heavy chain (KHC) and the kinesin light chain (KLC). To date the role of kinesin-1 in cancer including breast cancer has not been extensively studied. Furthermore, it is not known whether the role of kinesin in breast tumorigenesis is limited to its function as a motor protein.

Added value of this study

In this study, we found the subunits of kinesin-1, KIF5B and KLC1, to be critical regulators of EMP in breast cancer showing opposite roles. We found that KIF5B to be highly expressed in the most aggressive basal/claudin low TNBC breast cancer subtype and is essential for cell viability, migration, invasion, stemness, tumorigenesis and metastasis. In contrast, we found its classical partner protein KLC1 to be expressed in luminal/epithelial breast cancer cells and to possess anti-invasive activity. Importantly, we found that loss of KLC1 expression in luminal breast cancer subtypes resulted in nuclear accumulation of KIF5B and acquisition of mesenchymal, invasive and stem-like phenotype with loss of epithelial properties.

Implications of all the available evidence

This study revealed a new understanding of the role of kinesin-1 in breast cancer mediating EMP programing. Our results highlight for the first time a KIF5B/KLC1 switch regulating EMP in breast cancer that may prove useful for EMP-targeted therapies.

mesenchymal aggressive breast cancer subtypes represented by TNBC. Therefore, better understanding of molecular mechanisms that regulate EMP, and subsequently the critical switch/conversion of breast cancer cells from epithelial to acquiring mesenchymal and stem-like properties leading to tumor heterogeneity and aggressive phenotype may offer much needed new targets for prognosis and therapy in breast cancer.

Kinesin superfamily proteins (KIFs) are well known to be involved in intracellular movement and cytoplasmic transport of membranous organelles and macromolecules including complex proteins as well as RNA along the microtubules network. These superfamily proteins comprise 15 kinesin families termed kinesin-1 to kinesin-14B [9,10]. Each kinesin consists of a heterodimer complex of two subunits the kinesin heavy chain (KHC), mediating the motor function along the microtubules, and the kinesin light chain (KLC), recognizing cargoes and tethering them to KHC [11,12]. Kinesin-driven transport along microtubules is mediated by the concert function of both KHC and KLC subunits [10]. Kinesin-1 is the most studied family among kinesin proteins consisting of three types of KHC subunits (KIF5A, KIF5B and KIF5C) encoded by three different genes and four KLC subunits (KLC1–4) [13]. Studies have linked abnormalities in motor-driven transport to a wide range of diseases including cancer [10,14,15]. Kinesin family member 5B (KIF5B) is the most studied KHC subunit in kinesin-1 family and has been shown to be implicated in myogenesis, nuclear infusion and kidney development [16–18]. To date the role of kinesin-1 in cancer including breast cancer has not been extensively studied. Indeed, KIF5B has been shown to play a role in breast tumorigenesis through regulating transport of lysosomes, mitochondria and membrane-type 1 matrix metalloproteinase (MT1-MMP) contributing to cell migration [19–21]. Still however it is not known whether KIF5B role in breast tumorigenesis is limited to its function as a motor protein. As well, the role of its partner protein KLC in breast tumorigenesis is not yet elucidated.

In this study, we found KIF5B and KLC1, subunits of kinesin-1 to be critical regulators of EMP in breast cancer showing opposite roles. We found that KIF5B to be highly expressed in the most aggressive basal/claudin low TNBC subtype and is essential for cell viability, migration, invasion, stemness tumorigenesis and metastatic potential in this breast cancer subtype. Interestingly, we found atypical nuclear accumulation and interaction of KIF5B with the EMT inducer zinc finger transcription factor Snail 1 in basal/claudin low TNBC cells. In contrast, we found its classical partner protein KLC1 to be expressed in luminal/epithelial breast cancer cells and to possess anti-invasive activity. Importantly, we found that loss of KLC1 expression in luminal breast cancer subtypes resulted in nuclear accumulation of KIF5B and acquisition of mesenchymal, invasive and stem-like phenotype with loss of epithelial properties. Finally, we demonstrated that while KIF5B is required for the pro-invasive activity of TGF-β, we found the EMT suppressor PRL hormone to induce KIF5B/KLC1interaction and relocalization of KIF5B to the cytoplasm in basal/claudin low TNBC cells. Together, these results highlight for the first time a KIF5B/KLC1 switch regulating EMP in breast cancer that may prove useful for EMP-targeted therapies.

2. Results

2.1. Differential expression of KIF5B and its partner protein KLC1 in breast Cancer molecular subtypes

Based on microarray gene-profiling analysis of PRL-regulated mammary epithelial cellular differentiation program we have identified KIF5B to be a novel PRL down-regulated target gene [22]. As shown in Supplementary Fig. S1, while PRL treatment of the mammary luminal/epithelial HC11cells resulted in a significant decrease in KIF5B m-RNA levels, on the other hand, blocking PRLR signaling by suppressing expression of Jak2 [23], a major PRL downstream kinase, resulted in increased KIF5B expression both at the mRNA and protein levels. These results suggest that expression/activation of PRL/Jak2 signaling pathway leads to downregulation of KIF5B gene expression in mammary epithelial cells prompting us to investigate the role of KIF5B in breast tumorigenesis. To address the molecular role of KIF5B in breast cancer we examined the mRNA as well as the protein expression levels of KIF5B in breast cancer cells representative of the different clinically relevant breast cancer molecular subtypes, including luminal A (T47D and MCF7 cells), luminal B (BT474 cells), Her-2E (SKBR3 cells), triple negative (TN)-luminal-androgen receptor (LAR) (MDA-MB-453) and TN-basal-like/claudin low (MDA-MB-231, SCP2 and SUM159 cells) [24–26]. Interestingly, as shown in Fig. 1A, left panel, we found KIF5B m-RNA levels to be significantly higher in all breast cancer cells representative of the aggressive TN-basal-like/claudin low subtype, in comparison to the breast cancer cells representative of the TN-LAR (MDA-MB-453) which is characterized by a luminal-epithelial phenotype [8] as well as in breast cancer cells representative of the luminal A, luminal B and Her-2E subtypes. Similarly, as shown in Fig. 1A, right panel, KIF5B protein was readily detectable in all TN-basal-like/claudin low cells but not in breast cancer cells of epithelial/luminal subtypes. This data suggests a potential role for KIF5B in TN-basal-like/claudin low tumorigenesis.

The kinesin-1 proteins KIF5B and KLC1 work in concert to mediate intracellular cargo transport [27,28]. Having shown that KIF5B is upregulated in TN-basal-like/claudin low cells, we next examined the expression level of its partner protein KLC1. Interestingly, examining mRNA expression levels of KLC1 in the different breast cancer molecular subtypes showed a complete opposite pattern to that observed for KIF5B. Indeed, as shown in Fig. 1B, KLC1 is least expressed in the TN-basal-

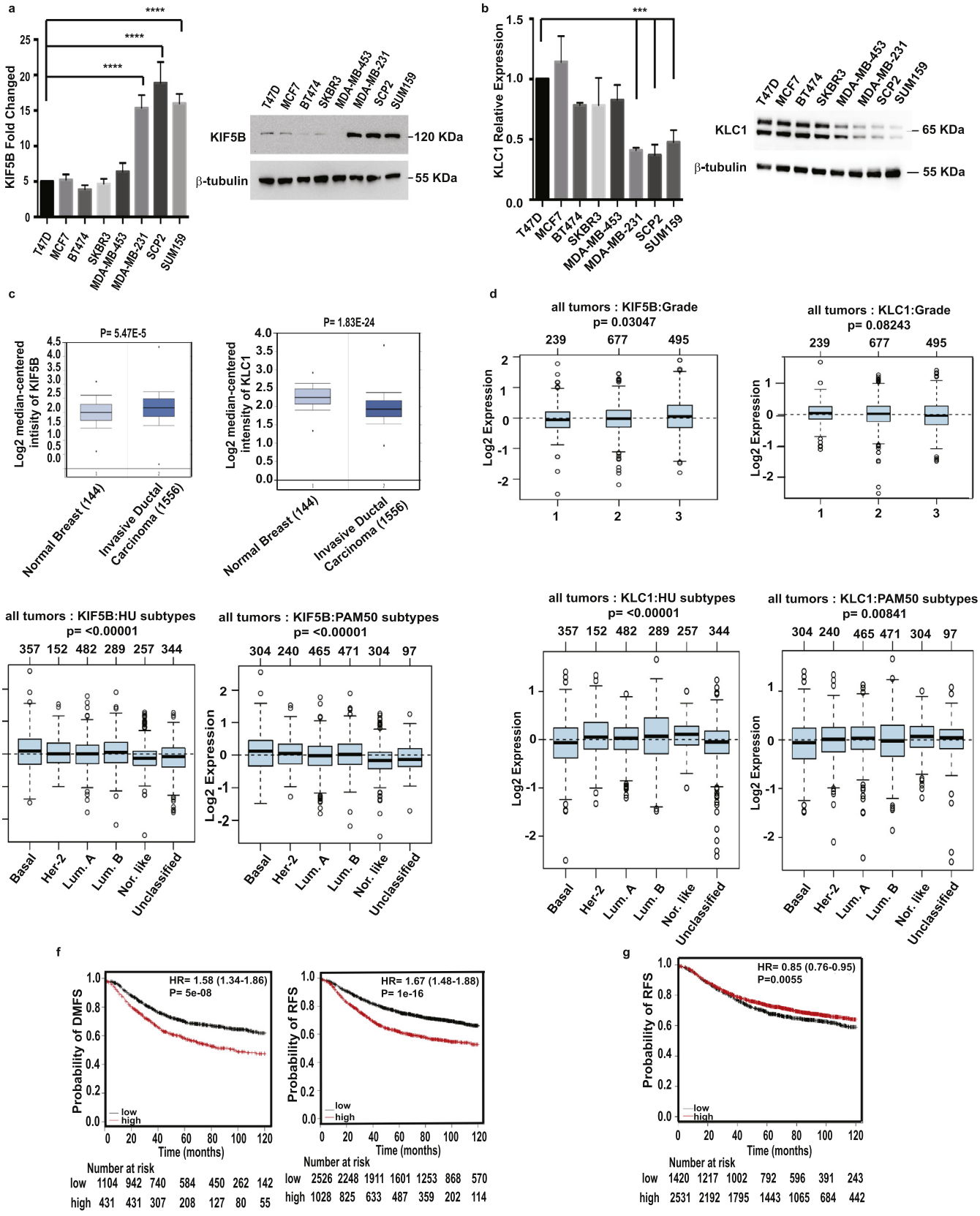
a
KIF5B Fold Changed
****
****
****
T47D MCF7 BT474 SKBR3 MDA-MB-453 MDA-MB-231 SCP2 SUM159
KIF5B
β-tubulin
120 KDa
55 KDa
b
KLC1 Relative Expression
***
KLC1
β-tubulin
65 KDa
55 KDa
c
P= 5.47E-5
Log2 median-centered intisity of KIF5B
P= 1.83E-24
Log2 median-centered intensity of KLC1
Normal Breast (144)
Invasive Ductal Carcinoma (1556)
d
all tumors : KIF5B:Grade
p= 0.03047
all tumors : KLC1:Grade
p= 0.08243
239 677 495
Log2 Expression
e
all tumors : KIF5B:HU subtypes
p= <0.00001
all tumors : KIF5B:PAM50 subtypes
p= <0.00001
all tumors : KLC1:HU subtypes
p= <0.00001
all tumors : KLC1:PAM50 subtypes
p= 0.00841
357 152 482 289 257 344
304 240 465 471 304 97
Basal Her-2 Lum. A Lum. B Nor. like Unclassified
f
Probability of DMFS
HR= 1.58 (1.34-1.86)
P= 5e-08
Probability of RFS
HR= 1.67 (1.48-1.88)
P= 1e-16
low
high
Time (months)
Number at risk
low 1104 942 740 584 450 262 142
high 431 431 307 208 127 80 55
low 2526 2248 1911 1601 1253 868 570
high 1028 825 633 487 359 202 114
g
HR= 0.85 (0.76-0.95)
P=0.0055
low 1420 1217 1002 792 596 391 243
high 2531 2192 1795 1443 1065 684 442

like/claudin low cells (MDA-MB-231, SCP2 and SUM159) in comparison to luminal A (T47D), luminal B (BT474), Her-2E (SKBR3) and TN-LAR (MDA-MB-453) cells both at the m-RNA and protein levels.

To further evaluate the role of Kinesin-1 components, KIF5B and KLC1 in breast cancer, we next examined their clinical significance using Curtis dataset, (ONCOMINE database) containing gene profiling data of 1700 breast cancer cases [29]. Interestingly, we found KIF5B mRNA levels to be significantly higher in invasive breast carcinoma (1556 cases) compared to normal breast tissue (144 cases) ($P = 5.47E-5$) (Fig. 1C, left panel). In contrast, KLC1 mRNA levels were found to be significantly lower in invasive breast carcinoma (1556 cases) compared to normal breast tissue (144 cases) ($P = 1.83E-24$) (Fig. 1C, right panel). We next examined the mRNA levels of KIF5B using a cohort of 1411 breast cancer cases in GOBO database. We found higher KIF5B mRNA levels in the poorly differentiated grade III tumors compared to grades II and I tumors while we found KLC1 mRNA levels to be higher in well differentiated grade I tumors compared to grade II and III with a *P* value of ($P = .03047$) and ($P = .08243$) respectively (Fig. 1D). Next, we examined KIF5B gene expression in relation to clinically relevant breast cancer molecular subtypes [30] in GOBO database (containing 1881 human breast cancer cases) using HU and PAM50 sub-classifications [31], we found KIF5B mRNA levels to be highest in the basal-like subtype and lowest in the luminal A subtype ($P \leq .00001$) (Fig. 1E, left panel). In contrast, we found that KLC1 mRNA levels to be highest in luminal subtypes and lowest in basal-like subtype, (Hu P ≤ .00001; PAM50 $P = .0084$) (Fig. 1E, right panel). Lastly, we analyzed the association between KIF5B mRNA levels and patient outcomes represented as distant metastasis free survival (DMFS) and relapse free survival (RFS). For these analyses we used Kaplan Meier plotter database which allow monitoring of survival of a large number of breast cancer patients for >10 years [32]. Interestingly, patients with higher KIF5B mRNA levels showed worse outcome presented as reduced DMFS and RFS (Fig. 1F). On the other hand, when analyzing the association between KLC1 mRNA levels and patient outcomes, we found that patients with higher KLC1 mRNA levels show significantly better RFS outcome (Fig. 1G) while there was no prognostic value for DMFS (Supplementary Fig. S3A). Taken together, these findings demonstrate that KIF5B and KLC1 are differentially expressed in the different clinically relevant breast cancer molecular subtypes and suggest that these two components of the kinesin-1 complex have independent and potentially opposite functions in breast cancer.

2.2. TN-basal-like/claudin low breast cancer cells show dependency on KIF5B for viability/metabolic activity and invasion activity

We next investigated the functional role of KIF5B in breast tumorigenesis by means of RNA interference, using two independent KIF5B-specific shRNAs in the TN-basal-like/claudin low MDA-MB-231 cells. Effectiveness of KIF5B knockdown was verified at both m-RNA and protein levels for each ShRNA (Fig. 2A). As can be seen in Fig. 2B, blocking KIF5B expression resulted in a significant loss of cell viability, most evident at 96 h time point. Our data also showed that KIF5B knockdown significantly decreased the migratory property of the MDA-MB-231 cells (Supplementary Fig. S2A). Moreover, KIF5B knockdown also resulted in a significant loss in the invasive capacity of the MDA-MB-231 cells (Fig. 2C). To avoid the limitation of a single cell line, these findings were reproduced in another aggressive TN-basal-like/claudin low cell model system SUM159, in which KIF5B was also found to be highly expressed and showed the same effects as that seen in MDA-MB-231 cells (Fig. 2D). Moreover, upon knockdown of KIF5B, we observed a change in cell morphology of the TN-basal-like/claudin low cells MDA-MB-231 and SUM159 from mesenchymal to cuboidal shape (Supplementary Fig. S2B). To further elaborate on the role of KIF5B in breast cancer, we suppressed KIF5B expression in the luminal A T47D cells normally expressing low levels of KIF5B. Interestingly, no change in cell viability or morphology was observed following KIF5B knockdown (Fig. 2E & Supplementary Fig. S2C). Altogether these results highlight a pro-oncogenic role for KIF5B in mediating cell viability, migration and invasion capacities in TN-basal-like/claudin low cells.

2.3. KIF5B plays a central role in inducing the EMT program, stemness and tumorigenic potential in TN-basal-like/claudin low cells

It is well known that the invasive capacity and distant metastasis properties of TN-basal-like/claudin low cells are mediated through acquisition of molecular signals that activate the function and/or expression of various EMT transcription factors and markers while suppressing the expression of epithelial markers [33,34]. To further decipher the role of KIF5B in breast cancer we then examined the role of KIF5B in regulating the EMT process. For this we examined the expression levels of EMT markers in MDA-MB-231 cells following knock-down of KIF5B. As shown in Fig. 3A, our data revealed that blocking KIF5B expression significantly decreased the m-RNA levels for several EMT transcription factors (ZEB1, ZEB2, Slug and Snail1) and mesenchymal markers (vimentin and FN1). Loss of protein expression levels of Snail-1, ZEB1 and vimentin were also confirmed by western blot and immunofluorescence analyses (Fig. 3B). On the other hand, loss of KIF5B resulted in a significant up-regulation in gene expression levels of the epithelial markers E-cadherin, CK18 as well as of the PRLR (Fig. 3C). The gain in E-cadherin and CK18 protein expression was further confirmed using western blot and immunofluorescence analyses (Fig. 3D). Importantly, our immunofluorescence data show that the re-expressed E-cadherin was not restricted only to the cell membrane but also associated with intracellular structures. Together, these results underscore the critical role of KIF5B in mediating induction of EMT reprograming and suppression of epithelial differentiation pathways in TN-basal-like/claudin low tumors.

Breast cancer stem-like cells (BCSCs) are largely responsible for the aggressive phenotype, high invasive capacity and high rate of recurrence in TN-basal-like/claudin low tumors. In particular, the $CD44^{high}/CD24^{low}$ stem-like cell sub-population has been identified as a mesenchymal-tumorigenic subpopulation with high metastatic activity [35–37]. We thus examined the role of KIF5B in regulating the stem cell phenotype of TN-basal-like/claudin low cells. Interestingly, loss of KIF5B expression in MDA-MB-231 cells resulted in a significant reduction in the stem-like cell sub-population $CD44^{+}/CD24^{-}$ with a significant increase in the number of the non-tumorigenic $CD44^{-}/CD24^{-}$ cell sub-population (Fig. 3E). Furthermore, examining individual stem cell

Fig. 1. KIF5B and KLC1 expression in relation to breast cancer molecular subtypes and patient outcome. A. Left panel, expression of KIF5B was examined using q-RT-PCR in T47D (control), MCF7, BT474, SKBR3, MDA-MB-453, MDA-MB-231, SCP2 and SUM159 cells. Results are expressed as relative expression of triplicates of three independent experiments $^{****}p \leq .0001$ (one-way ANOVA). Right panel, T47D, MCF7, BT474, SKBR3, MDA-MB-453, MDA-MB-231, SCP2 and SUM159 cells were lysed and western blotting was carried out using monoclonal antibodies against KIF5B and β-tubulin. B. Left panel, m-RNA levels of KLC1 using q-RT-PCR in T47D (control), MCF7, BT474, SKBR3, MDA-MB-453, MDA-MB-231, SCP2 and SUM159. Results are expressed as relative expression of triplicates of three independent experiments $^{***}p \leq .001$ (one-way ANOVA). Right panel, immunoblot analysis of total cell lysates of breast cancer cells using monoclonal antibodies against KLC1 and β-tubulin. C. KIF5B (left panel) and KLC1 (right panel) mRNA expression levels in 144 normal and 1556 invasive breast cancer cases using Curtis dataset of ONCOMINE database. D. KIF5B (left panel) and KLC1 (right panel) mRNA expression levels stratified according to tumor grade in a cohort of 1411 cases using GOBO database. E. KIF5B (left panel) and KLC1 (right panel) mRNA expression levels in association with breast cancer molecular subtypes stratified according to Hu et al. as well as PAM50 sub-classification methods in 1881 human breast cancer samples using GOBO database. F. Kaplan-Meier survival curves of KIF5B gene expression in association with patient outcome (1535 patients, KM-plotter database) using DMFS as an end point (left panel). Kaplan-Meier survival curves of KIF5B gene expression in association with patient outcome (3554 patients, KM-plotter database) using RFS as an end point (middle panel). G. Kaplan-Meier survival curves of KLC1 gene expression in association with patient outcome (3951 patients, KM-plotter database) using RFS as an end point.

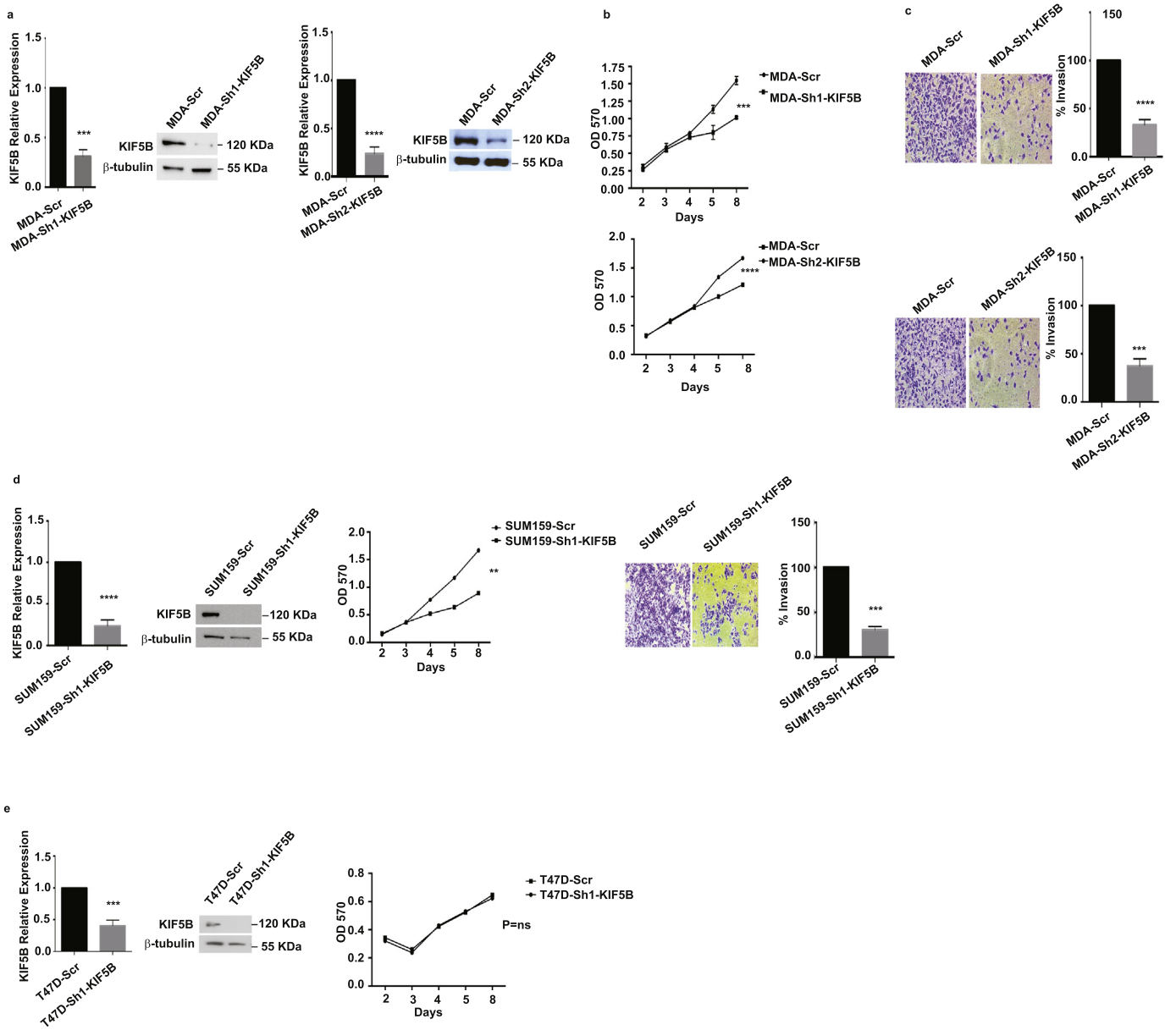

Fig. 2. KIF5B is required for TN-basal-like/claudin low cell viability and invasion capacity. A. Left panel, m-RNA levels of KIF5B were assessed using q-RT-PCR in MDA-MB-231-Scr (control) & MDA-MB-231-Sh1-KIF5B cells. Results are expressed as relative expression of triplicates of three independent experiments $^{***}p < .001$ (Student's *t*-test). Immunoblot analysis of total cell lysates of MDA-MB-231-Scr (control) & MDA-MB-231-Sh1-KIF5B cells using antibodies against KIF5B and β-tubulin. Right panel, m-RNA levels of KIF5B were assessed using q-RT-PCR in MDA-MB-231-Scr (control) & MDA-MB-231-Sh2-KIF5B cells. Results are expressed as relative expression of triplicates of three independent experiments $^{****}p < .0001$ (Student's *t*-test). Immunoblot analysis of total cell lysates of MDA-MB-231-Scr (control) & MDA-MB-231-Sh2-KIF5B cells using antibodies against KIF5B and β-tubulin. B. MTT assays were performed in MDA-MB-231-Scr & MDA-MB-231-Sh1-KIF5B (upper panel) and in MDA-MB-231-Scr & MDA-MB-231-Sh2-KIF5B (lower panel) for 2, 3, 4, 5 and 8 days. Results are expressed as mean ± SEM of triplicates of three independent experiments. $^{***}p \le .001$, $^{****}p < .0001$ (one-way ANOVA). C. Quantitative invasion assays of MDA-MB-231-Scr and MDA-MB-231-Sh1-KIF5B (upper panel) and MDA-MB-231-Scr and MDA-MB-231-Sh2-KIF5B (lower panel). Results presented are of triplicates of three independent experiments $^{****}p < .0001$. $^{***}p \le .001$ (Student's *t*-test). D. m-RNA levels of KIF5B were assessed using q-RT-PCR in SUM159-Scr (control) & SUM159-Sh1-KIF5B cells (left panel). Immunoblot analysis of total cell lysates of SUM159-Scr (control) & SUM159-Sh-KIF5B cells using antibodies against KIF5B and β-tubulin (right panel). E. Left panel, MTT assays were performed in SUM159-Scr & SUM159-Sh1-KIF5B for 2, 3, 4, 5 and 8 days. Right panel, quantitative invasion assays of SUM159-Scr and SUM159-Sh1-KIF5B. Results are expressed as mean ± SEM of triplicates of three independent experiments $^{****}p < .0001$, $^{***}p \le .0001$ and $^{**}p \le .01$ (one-way ANOVA). F. Left panel, m-RNA levels of KIF5B were assessed using q-RT-PCR in T47D-Scr (control) & T47D-Sh1-KIF5B cells. Results are expressed as relative expression of triplicates of three independent experiments $^{***}p < .001$ (Student's *t*-test). Middle panel, immunoblot analysis of total cell lysates of T47D-Scr (control) & T47D-Sh1-KIF5B cells using antibodies against KIF5B and β-tubulin. Right panel, MTT assays were performed in T47D-Scr & T47D-Sh1-KIF5B for 2, 3, 4, 5 and 8 days. Results are expressed as mean ± SEM of triplicates of three independent experiments. ns: non-significant (one-way ANOVA)

marker expression level, we found that loss of KIF5B led to a significant decrease in CD44 but not CD24 m-RNA levels (Fig. 3F). This was followed by a significant decrease in gene expression levels of the self-renewal transcriptional factors OCT4, NANOG and SOX2 (Fig. 3G). Next, we assessed the overall effect of loss of KIF5B expression on the tumorigenic capacity of MDA-MB-231 cells using colony formation assay. As shown Fig. 3H, loss of KIF5B expression resulted in a significant decrease of the clonogenic capacity of MDA-MB-231 cells. On the other hand, there was no effect of loss of KIF5B on the clonogenic capacity of the luminal A T47D cells (Supplementary Fig. S2B). We then tested the effect of loss of KIF5B in modulating BCSC self-renewal, using tumorsphere formation assays. MDA-Scr and MDA-KIF5BShRNA cells were seeded at 1000, 500, 100, 50, 10 and 1 cells/well and tumorsphere formation was monitored. While we observed no differences in tumorsphere formation capacity between MDA-Scr and MDA-KIF5BShRNA cells at 1000 and 500 cells/well, we found a significant

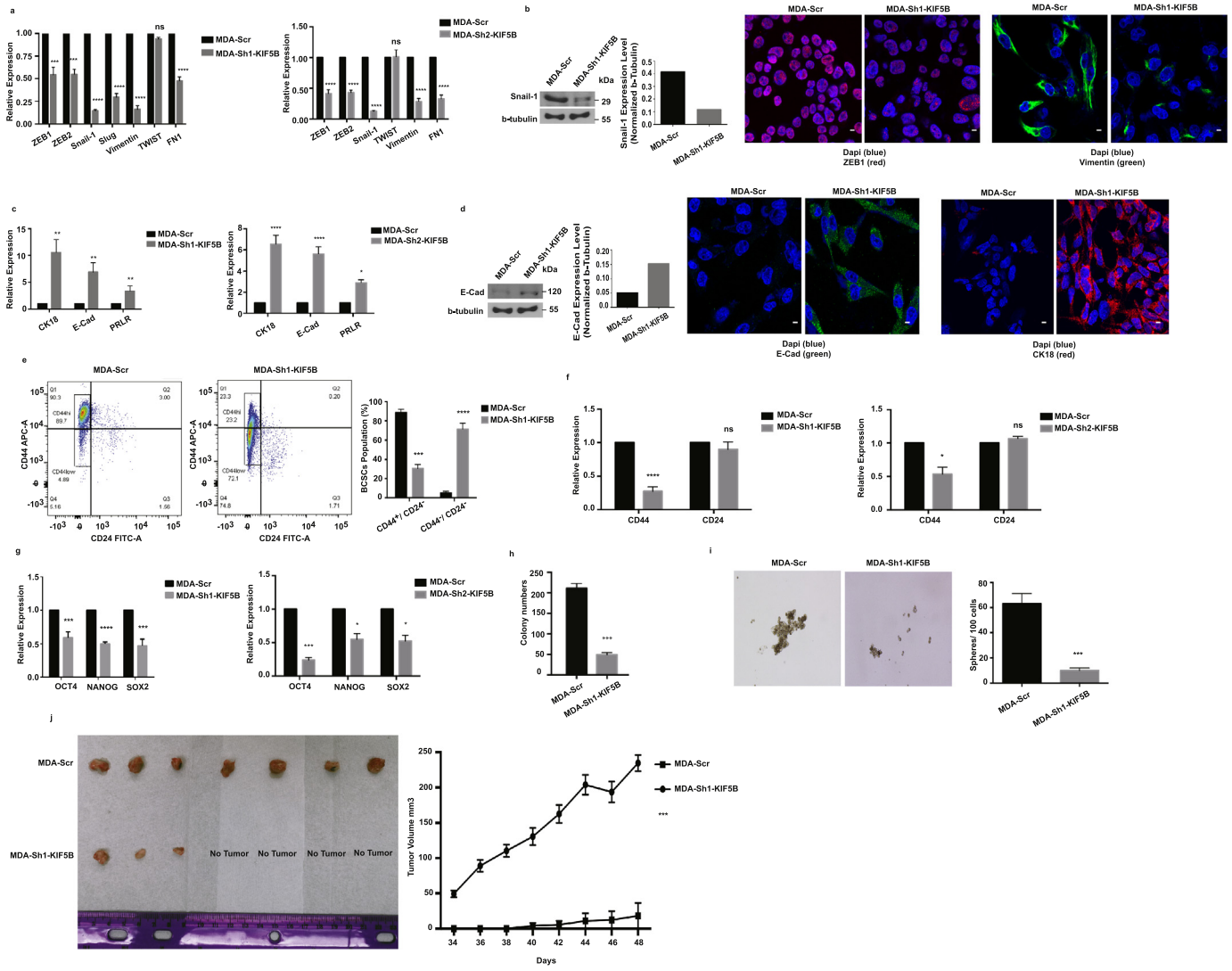

Fig. 3. KIF5B is required for EMT programing and stemness in TN-basal-like/claudin low cells. A. Left and right panels, m-RNA expression levels of EMT transcription factors and markers using q-RT-PCR in both MDA-MB-231-Scr & MDA-MB-231-Sh1-KIF5B and MDA-MB-231-Scr & MDA-MB-231-Sh2-KIF5B. Results are expressed as relative expression of triplicates of three independent experiments $^{****}p \leq .0001$, $^{***}p \leq .001$ and ns: not significant (one-way ANOVA). B. Left panel, immunoblot analysis of total cell lysates of MDA-MB-231-Scr (control) & MDA-MB-231-Sh1-KIF5B cells using antibodies against Snail1 and β-tubulin. Middle panel, confocal immunofluorescence images ZEB1 (red) and nucleus (Dapi) (blue) of MDA-MB-231-Scr (control) & MDA-MB-231-Sh1-KIF5B cells. Scale bar, 10 μm. Right panel, confocal immunofluorescence images Vimentin (green) and nucleus (Dapi) (blue) of MDA-MB-231-Scr (control) & MDA-MB-231-Sh1-KIF5B cells. Scale bar, 10 μm. C. Left and right panels, m-RNA expressions levels of epithelial markers CK18, E-cadherin and PRLR using q-RT-PCR in MDA-MB-231-Scr & MDA-MB-231-Sh1-KIF5B and MDA-MB-231-Scr & MDA-MB-231-Sh2-KIF5B. Results are expressed as relative expression of triplicates of three independent experiments $^{****}p \leq .0001$, $^{**}p \leq .01$ and $^{*}p \leq .05$ (Student's *t*-test). D. Left panel, immunoblot analysis of total cell lysates of MDA-MB-231-Scr (control) & MDA-MB-231-Sh1-KIF5B cells using antibodies against E-cadherin and β-tubulin. Middle panel, confocal immunofluorescence images E-cad (green) and nucleus (Dapi) (blue) of MDA-MB-231-Scr (control) & MDA-MB-231-Sh1-KIF5B cells. Scale bar, 10 μm. Right panel, confocal immunofluorescence images CK18 (red) and nucleus (Dapi) (blue) of MDA-MB-231-Scr (control) & MDA-MB-231-Sh1-KIF5B cells. Scale bar, 10 μm. E. The percentage content of breast CSCs ($CD44^{+}/CD24^{-/low}$) in MDA-MB-231-Scr and MDA-MB-231-Sh1-KIF5B were determined by flow cytometry (representative image of dot plot). Quantification analysis of three independent experiments expressed as mean ± SEM of triplicates of three independent experiments $^{****}p \leq .0001$ and $^{***}p \leq .001$ (Student's *t*-test). F. m-RNA levels of breast stem cell markers CD44 and CD24 were examined using q-RT-PCR in MDA-MB-231-Scr & MDA-MB-231-Sh1-KIF5B (left panel) and MDA-MB-231-Scr & MDA-MB-231-Sh2-KIF5B (right panel). Results are expressed as relative expression of triplicates of three independent experiments $^{****}p \leq .0001$, $^{*}p \leq .05$ and ns: not significant (Student's *t*-test). G. m-RNA levels of breast cancer stem cell self-renewal markers OCT4, NANOG and SOX2 were examined using q-RT-PCR in MDA-MB-231-Scr & MDA-MB-231-Sh1-KIF5B and MDA-MB-231-Scr & MDA-MB-231-Sh2-KIF5B. Results are expressed as relative expression of triplicates of three independent experiments $^{****}p \leq .0001$, $^{***}p \leq .001$ and $^{*}p \leq .05$ (Student's *t*-test). H. Colony formation assays were performed using MDA-MB-231-Scr & MDA-MB-231-Sh1-KIF5B for a period of three weeks. Results are expressed as mean ± SEM of triplicates of three independent experiments $^{***}p \leq .001$ (Student's *t*-test). I. Tumorsphere assays were performed using MDA-MB-231-Scr & MDA-MB-231-Sh1-KIF5B for a period of 7 days. Results are expressed as mean ± SEM of triplicates of three independent experiments $^{***}p \leq .001$ (Student's *t*-test). J. Left panel, images of MDA-Scr and MDA-Sh1-KIF5B tumors of NSG xenografts. Right panels, tumor volume measurements of NSG xenografts of MDA-Scr and MDA-Sh1-KIF5B followed for a period of 48 days.

loss of tumorsphere number in MDA-KIF5BShRNA cells in comparison to MDA-Scr cells starting at 100 cells/well (Fig. 2I). Next To address the role of KIF5B in driving breast tumorigenesis, we next examined the effects of loss of KIF5B expression on the tumorigenic potential of MDA-MB-231 cells using a mammary fat-pad orthotopic mouse model. While all mice injected with the control MDA-MB-231 cells expressing the scrambled ShRNA developed large tumors within the mammary fat-pad, only (3/7) mice injected with MDA-MB-231 cells expressing the KIF5B specific ShRNA developed tumors that were also significantly smaller than MDA-MB-231/Scr tumors (Fig. 3J). Together, these results clearly demonstrate a critical role for KIF5B in breast tumorigenesis generating a mesenchymal and stem-like phenotype characteristics of EMP and the aggressive TN-basal-like/claudin low phenotype.

2.4. KLC1 is required to maintain an epithelial and non-invasive breast Cancer phenotype

To address the role of KIF5B partner protein, KLC1, in breast cancer, we next suppressed KLC1 expression in the luminal A (T47D) and Her-2E (SKBR3) cells, using specific KLC1 siRNA (Fig. 4A). While knocking down KLC1 expression did not affect T47D and SKBR3 cell viability (Fig. 4B), importantly, we found that loss of KLC1 in T47D and SKBR3 cells reprogramed the normally non-invasive cells to an invasive phenotype (Fig. 4C). Furthermore, suppression of KLC1 resulted in a pronounced increase in expression of the EMT markers (ZEB1, ZEB2, Snail1, Slug, Vimentin and FN1) in the two epithelial/luminal breast cancer subtypes (Fig. 4D). The gain in expression of the EMT markers, Snail-1 and ZEB1, was also confirmed by immunofluorescence analyses (Fig. 4E). On the other hand, loss of KLC1 resulted in a significant down-regulation of m-RNA levels of the epithelial markers E-cadherin and the PRLR (Fig. 4F). Loss of E-cadherin protein expression level of was also confirmed by immunofluorescence analysis (Fig. 3G). Next, examining individual stem cell marker expression levels, we found that loss of KLC1 led to a significant increase in CD44 m-RNA level while CD24 m-

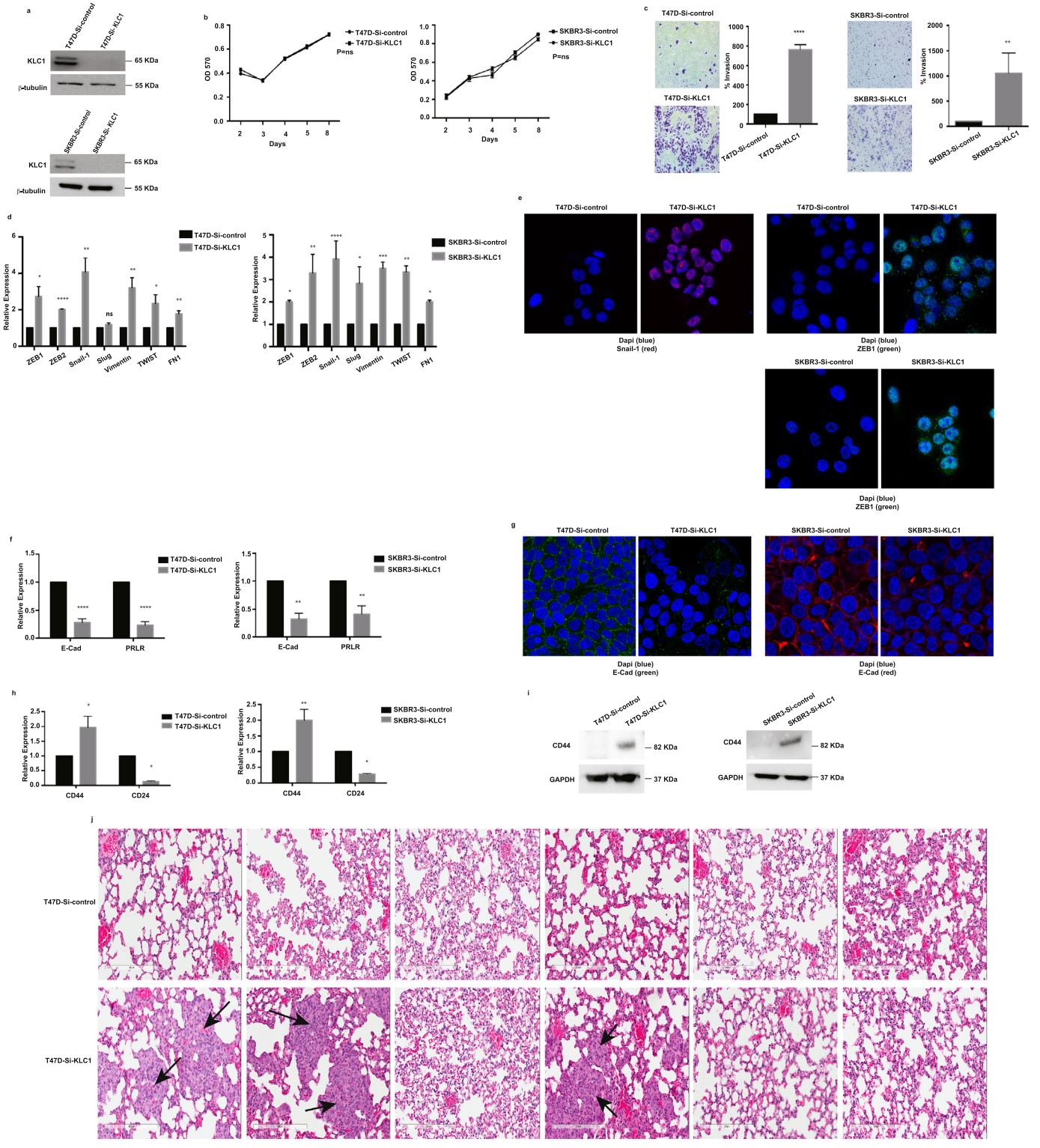

RNA level was significantly decreased (Fig. 4H). The gain in protein expression of CD44 marker was further confirmed using western blot analyses in T47D and SKBR3 cells (Fig. 4I). To rule out off-target effects of the siRNA, the above findings were reproduced using another siRNA targeting KLC1 in luminal A (T47D) cells (Supplementary Fig. S3).

The above data implicated KLC1 in maintaining a non-invasive epithelial phenotype in breast cancer cells. Therefore, next we examined the overall effect of loss of KLC1 in driving organ metastasis and lung colonization *in vivo*. For this, we assessed the effects of loss of KLC1 gene expression on lung metastasis using tail vein injection preclinical xenograft mouse model. Interestingly, while none of the 6 mice injected with the control T47D cells expressing the control siRNA developed lung micrometastases, 3/6 mice injected with T47D-Si-KLC1 cells developed lung metastasis (Fig. 4J) supporting a role for KLC1 in suppressing metastasis *in vivo*. Together, these results demonstrate a role for KLC1 in maintaining non-invasive epithelial phenotype in breast cancer cells. Altogether, these findings highlight a clear association between KLC1 expression and maintenance of an epithelial, non-invasive and non-metastatic cellular phenotype emphasizing an EMP suppressor role for KLC1 in breast cancer contrary to KIF5B.

2.5. Nuclear accumulation of KIF5B and KIF5B/SNAIL interaction in TN-basal-like/claudin low cells independent of KLC1

Having found a new role for KIF5B in promoting EMP, independent of KLC1, this prompted us to investigate whether KIF5B plays a nuclear role in breast cancer. Therefore, next we examined the subcellular localization of KIF5B in the different breast cancer molecular subtypes, using immunoblotting of nuclear fractions. Interestingly, as shown in Fig. 5A, we found high nuclear accumulation of KIF5B in the TN-basal-like/claudin low cells (MDA-MB-231, SCP2 and SUM159) while no nuclear signal for KIF5B could be detected in the epithelial/luminal breast cancer cells. In contrast, we could not detect any KLC1 nuclear accumulation in all breast cancer cell types. Moreover, immunofluorescence analysis of KIF5B showed strong nuclear localization of KIF5B in TNBC MDA-MB-231cells, while remaining unfocalized in luminal A T47D cells (Fig. 5B). In contrast, KLC1 showed cytoplasmic localization in both T47D and MDA-MB-231 cells (Fig. 5C). To investigate whether the nuclear accumulation of KIF5B is determined by KLC1 expression levels, we examined KIF5B nuclear levels following suppression of KLC1 expression in the luminal breast cancer cells T47D and Her-2E SKBR3 cells. We examined KIF5B nuclear levels following suppression of KLC1 expression in the luminal breast cancer cells T47D and Her-2E SKBR3 cells. Interestingly, loss of KLC1 expression in the two luminal molecular subtypes led to KIF5B nuclear accumulation while no change in total KIF5B expression level was observed (Fig. 5D), suggesting that KLC1 expression levels influence and control KIF5B nuclear localization. These results highlight a potential nuclear function for KIF5B in TN-basal-like/claudin low cells deriving EMP independent of KLC1.

Next, we examined whether this nuclear accumulation of KIF5B in TN-basal-like/claudin low cells permits a new function for KIF5B in the nucleus. Therefore, we examined whether there is a physical interaction between KIF5B and the transcriptional regulators of EMT in TN-basal-like/claudin low cells. Indeed, as can be seen in Fig. 5E, all TN-basal-like/claudin low cells, MDA-MB-231, SCP2 and SUM159, showed KIF5B interaction with Snail1. Screening the possible interaction between KIF5B and transcription factors ZEB1, ZEB2 as well as Slug, our data did not detect any interaction between KIF5B and these proteins (data not shown). To address whether KIF5B regulates Snail1 function, we examined Snail1 nuclear localization in MDA-MB-231 cells following loss of KIF5B expression. Interestingly, as can be seen in Fig. 5F, MDA-MB-231-Sh1-KIF5B cells showed loss of Snail1 nuclear accumulation and its re-localization to the cytoplasm, highlighting an important function for KIF5B in regulating Snail1 nuclear accumulation in TN-basal-like/claudin low cells. Next, to investigate whether Snail1 exerts any regulatory role in KIF5B function, we suppressed Snail1 expression in MDA-MB-231 cells using a specific Snail1 siRNA (Supplementary Fig. S4A, left panel). As can be seen in Supplementary Fig. S4A right panel, no change in the nuclear accumulation of KIF5B was observed. Altogether, these findings indicate that KIF5B nuclear accumulation in breast cancer is context dependent and is regulated by the expression of KLC1 promoting EMT transcriptional programing.

2.6. KIF5B is essential for metastatic colonization propensity and is a clinically relevant marker of high-grade invasive breast cancer

The above data suggested that KIF5B is a critical inducer of EMT, stemness and invasion in breast cancer cells. Therefore, next we examined the role of KIF5B in driving organ metastasis *in vivo*. For this, we monitored the effects of loss of KIF5B gene expression on lung metastasis using tail vein injection preclinical xenograft mouse model. Remarkably, while 6 out of 6 mice injected with the control MDA-MB-231 cells expressing the scrambled shRNA developed lung macrometastases, none of the 6 mice injected with MDA-MB-231-Sh1KIF5B cells developed lung metastasis (Fig. 6A). These results demonstrate that KIF5B is a driver of metastatic colonization, the functional endpoint of EMP.

As cancer cells adopt the EMP programing and invasive/metastatic behavior, they acquire cellular features clinically associated with high-grade invasive malignancy [38,39]. Next, we investigated the clinical features of breast cancer cases expressing KIF5B protein. For this, we used a TMA of 102 cases including 97 breast cancer cases and 5 normal/benign breast tissues. Importantly, we found KIF5B protein expression to be significantly higher in invasive ductal carcinoma in comparison to *in situ* carcinoma ($p = .04$). We then investigated whether KIF5B expression correlated with the different molecular and histological subtypes of breast cancer. We found a trend of high KIF5B protein expression in triple negative molecular subtype of breast cancer. Moreover, KIF5B protein expression was associated with poorly differentiated tumors (grade III) (81.25%) in comparison to the moderately

Fig. 4. Loss of KLC1 expression in breast cancer cells induces aggressive phenotype. A. Immunoblot analysis of total cell lysates of T47D-Si-control and T47D-Si-KLC1 (upper panel) and of SKBR-Si-control and SKBR-Si-KLC1 (lower panel) using monoclonal antibodies against KLC1 and β-tubulin. B. MTT assays of T47D- Si-control and T47D-Si-KLC1 (left panel) and of SKBR-Si-control and SKBR-Si-KLC1 (right panel) for 2, 3, 4, 5 and 8 days. Results are expressed as mean ± SEM of triplicates of three independent experiments. ns: non significant (one-way ANOVA). C. Quantitative invasion assay of T47D- Si-control and T47D-Si-KLC1 (left panel) and SKBR3-Si-control & SKBR3-Si-KLC1 (right panel). Results are expressed as relative expression of triplicates of three independent experiments $^{****}p \le .0001$ and $^{**}p \le .01$ (Student's *t*-test). D. m-RNA levels of EMT transcription factors and markers ZEB1, ZEB2, Snail1, Slug, Vimentin, TWIST and FN1 using q-RT-PCR in T47D- Si-control & T47D-Si-KLC1 (left panel) and SKBR3-Si-control & SKBR3-Si-KLC1 (right panel). Results are expressed as relative expression of triplicates of three independent experiments $^{****}p \le .0001$, $^{***}p \le .001$, $^{**}p \le .01$, $^{*}p \le .05$ and ns: non significant (Student's *t*-test). E. Left panel, confocal immunofluorescence images Snail-1 (red) and nucleus (Dapi) (blue) of T47D-Si-control & T47D-Si-KLC1 cells. Scale bar, 10 μm. Upper right panel, confocal immunofluorescence images ZEB1 (green) and nucleus (Dapi) (blue) of T47D-Si-control & T47D-Si-KLC1 cells. Scale bar, 10 μm. Lower right panel, confocal immunofluorescence images ZEB1 (green) and nucleus (Dapi) (blue) SKBR3-Si-control & SKBR3-Si-KLC1 cells. Scale bar, 10 μm. F. m-RNA expressions levels of epithelial markers E-cadherin and PRLR using q-RT-PCR in T47D- Si-control & T47D-Si-KLC1 (left panel) and SKBR3-Si-control & SKBR3-Si-KLC1 (right panel). Results are expressed as relative expression of triplicates of three independent experiments $^{****}p \le .0001$ and $^{**}p \le .01$ (Student's *t*-test). G. Left panel, confocal immunofluorescence images E-cadherin (green) and nucleus (Dapi) (blue) of T47D-Si-control & T47D-Si-KLC1 cells. Scale bar, 10 μm. Right panel, confocal immunofluorescence images E-cadherin (red) and nucleus (Dapi) (blue) SKBR3-Si-control & SKBR3-Si-KLC1 cells. Scale bar, 10 μm. H. m-RNA levels of breast stem cell markers CD44 and CD24 were examined using q-RT-PCR in T47D- Si-control & T47D-Si-KLC1 (left panel) and SKBR3-Si-control & SKBR3-Si-KLC1 (right panel). Results are expressed as relative expression of triplicates of three independent experiments $^{**}p \le .01$ and $^{*}p \le .05$ (Student's *t*-test). I. Immunoblot analysis of total cell lysates of T47D-Si-control and T47D-Si-KLC1 (left panel) and of SKBR-Si-control and SKBR-Si-KLC1 (right panel) using monoclonal antibodies against CD44 and β-tubulin. J. Representative gross photo of lungs as well as H& E histological images of NSG tail vein mouse xenografts of T47D-Si-control and T47D-Si-KLC1. Black arrow heads indicate micrometastasis.

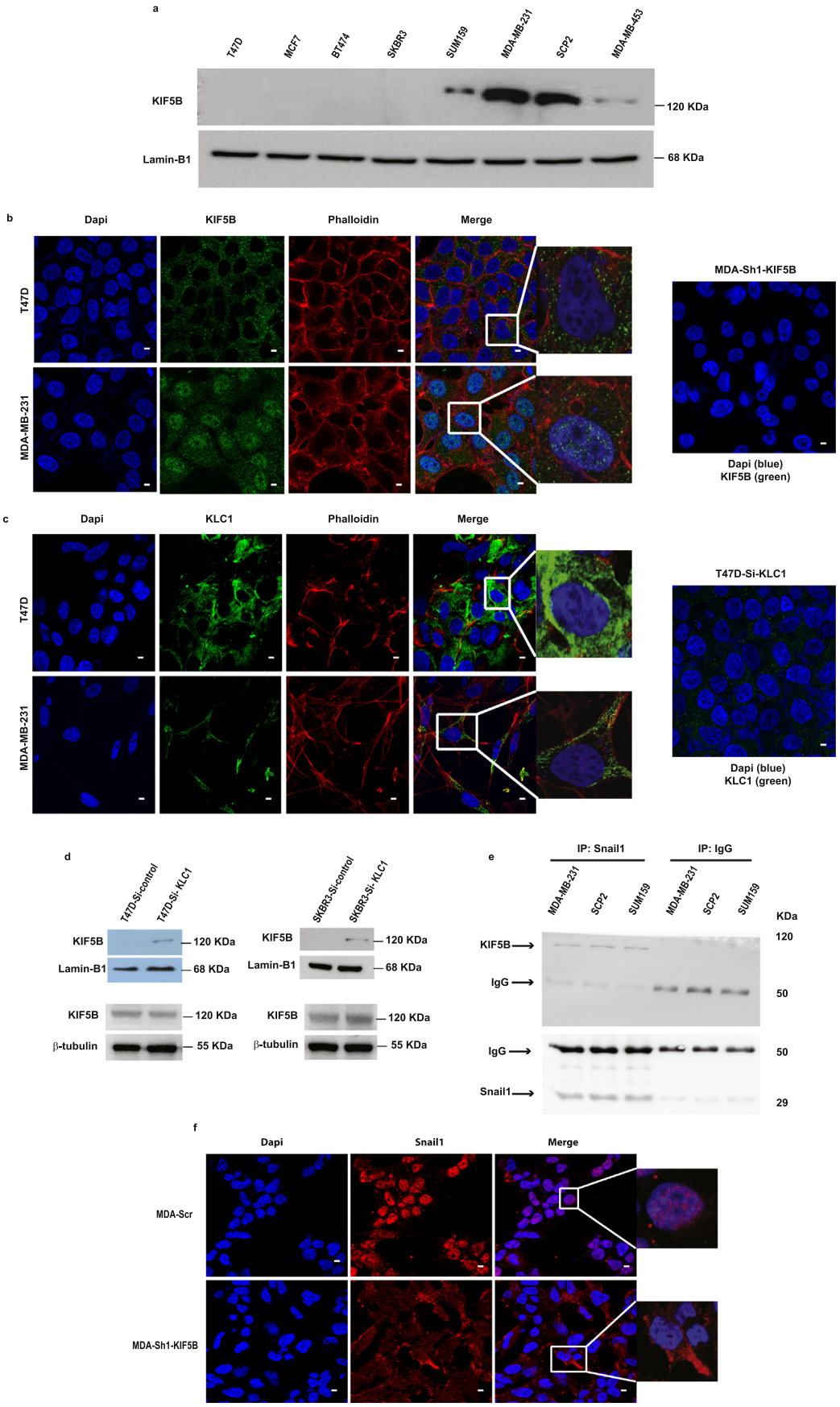
a
T47D
MCF7
BT474
SKBR3
SUM159
MDA-MB-231
SCP2
MDA-MB-453
KIF5B
120 KDa
Lamin-B1
68 KDa
b
Dapi
KIF5B
Phalloidin
Merge
T47D
MDA-MB-231
MDA-Sh1-KIF5B
Dapi (blue)
KIF5B (green)
c
Dapi
KLC1
Phalloidin
Merge
T47D
MDA-MB-231
T47D-Si-KLC1
Dapi (blue)
KLC1 (green)
d
T47D-Si-control
T47D-Si- KLC1
SKBR3-Si-control
SKBR3-Si- KLC1
KIF5B
120 KDa
Lamin-B1
68 KDa
β-tubulin
55 KDa
e
IP: Snail1
IP: IgG
MDA-MB-231
SCP2
SUM159
KDa
120
50
29
KIF5B
IgG
Snail1
f
Dapi
Snail1
Merge
MDA-Scr
MDA-Sh1-KIF5B

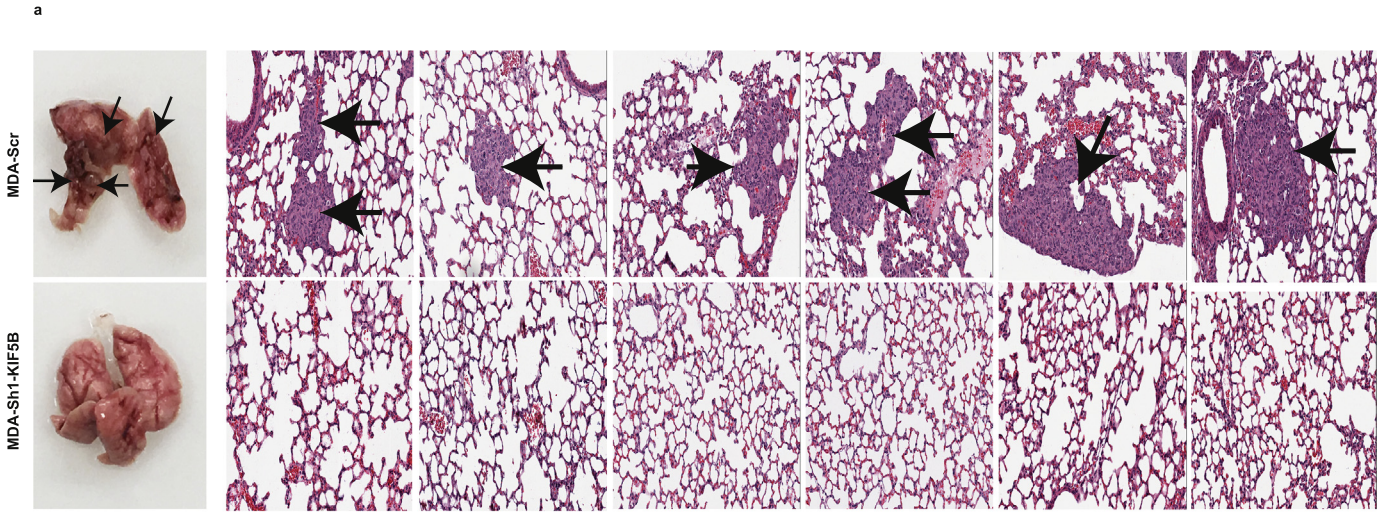

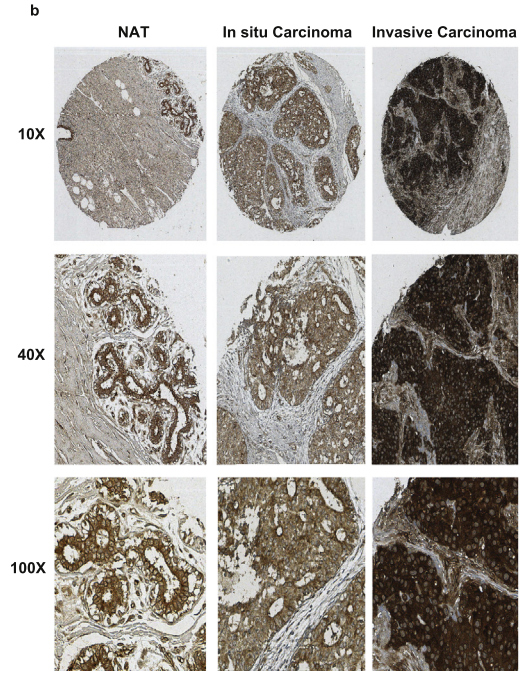

Pathology	Negative	Positive	Total	%	P-value
Normal/Benign	4	1	5	20.00	
IN situ	5	1	6	16.67	0.045298
Invasive	38	52	90	57.78	
Histological type	Negative	Positive	Total		
Molecular subtype	Negative	Positive	Total		
Luminal A	8	12	20	60.00	
Luminal B	10	14	24	58.33	
Her-2	12	14	26	53.85	
Triple negative	3	7	10	70.00	0.144
Grade	Negative	Positive	Total		
I	13	6	19	31.58	
II	21	32	53	60.38	0.01
III	3	13	16	81.25	

Fig. 6. Breast cancer shows dependency on KIF5B for invasive capacity and metastasis in preclinical mouse model. A. Representative gross photo of lungs as well as H& E histological images of NOD-SCID tail vein mouse xenografts of MDA-MB-231-Scr MDA-MB-231-Sh-KIF5B. Black arrow heads indicate macro and micrometastasis. B. Left panel, positive immunohistochemical staining of KIF5B in normal adjacent tissue, *in situ* and invasive breast cancer lesions (10X and 40X). Right panel, associations between KIF5B protein expression and different clinicopathological parameters.

Fig. 5. KIF5B shows high nuclear accumulation and interaction with Snail1 in TN-basal-like/claudin low cells. A. Immunoblot analysis of nuclear extracts of breast cancer cells using monoclonal antibodies against KIF5B and Lamin-B1. B. Left panel, confocal immunofluorescence images of KIF5B (green), phalloidin (red) and nucleus (Dapi) (blue) of T47D (upper panel) & MDA-MB-231 (lower panel) cells. Scale bar, 10 μm. Right panel, confocal immunofluorescence images of KIF5B (green) and nucleus (Dapi) (blue) of MDA-Sh1-KIF5B cells (negative control). Scale bar, 10 μm. C. Left panel, confocal immunofluorescence images of KLC1 (green), phalloidin (red) and nucleus (Dapi) (blue) of T47D (upper panel) & MDA-MB-231 (lower panel) cells. Scale bar, 10 μm. Right panel, confocal immunofluorescence images of KLC1 (green) and nucleus (Dapi) (blue) of T47D-Si-KLC1 cells (negative control). Scale bar, 10 μm. D. Left panel, immunoblot analysis of nuclear extracts of T47D-Si-control (control) and T47D-Si-KLC1 (upper panel) and immunoblot analysis of total cell lysates of T47D-Si-control and T47D-Si-KLC1 (lower panel) using monoclonal antibodies against KIF5B, Lamin-B1 and β-tubulin. Right panel, immunoblot analysis of nuclear extracts of SKBR-Si-control and SKBR-Si-KLC1 (upper panel) and immunoblot analysis of total cell lysates of SKBR-Si-control and SKBR-Si-KLC1 (lower panel) using monoclonal antibodies against KIF5B, Lamin-B1 and β-tubulin. E. MDA-MB-231, SCP2 and SUM159 cells were lysed and immunoprecipitations were performed using a goat polyclonal antibody against Snail1 or control normal goat IgG. Western blotting was carried out using a rabbit monoclonal antibody against KIF5B. F. Confocal immunofluorescence images of Snail1 (red) and nucleus (Dapi) (blue) of MDA-MB-231-Scr (control) & MDA-MB-231-Sh1-KIF5B cells. Scale bar, 10 μm.

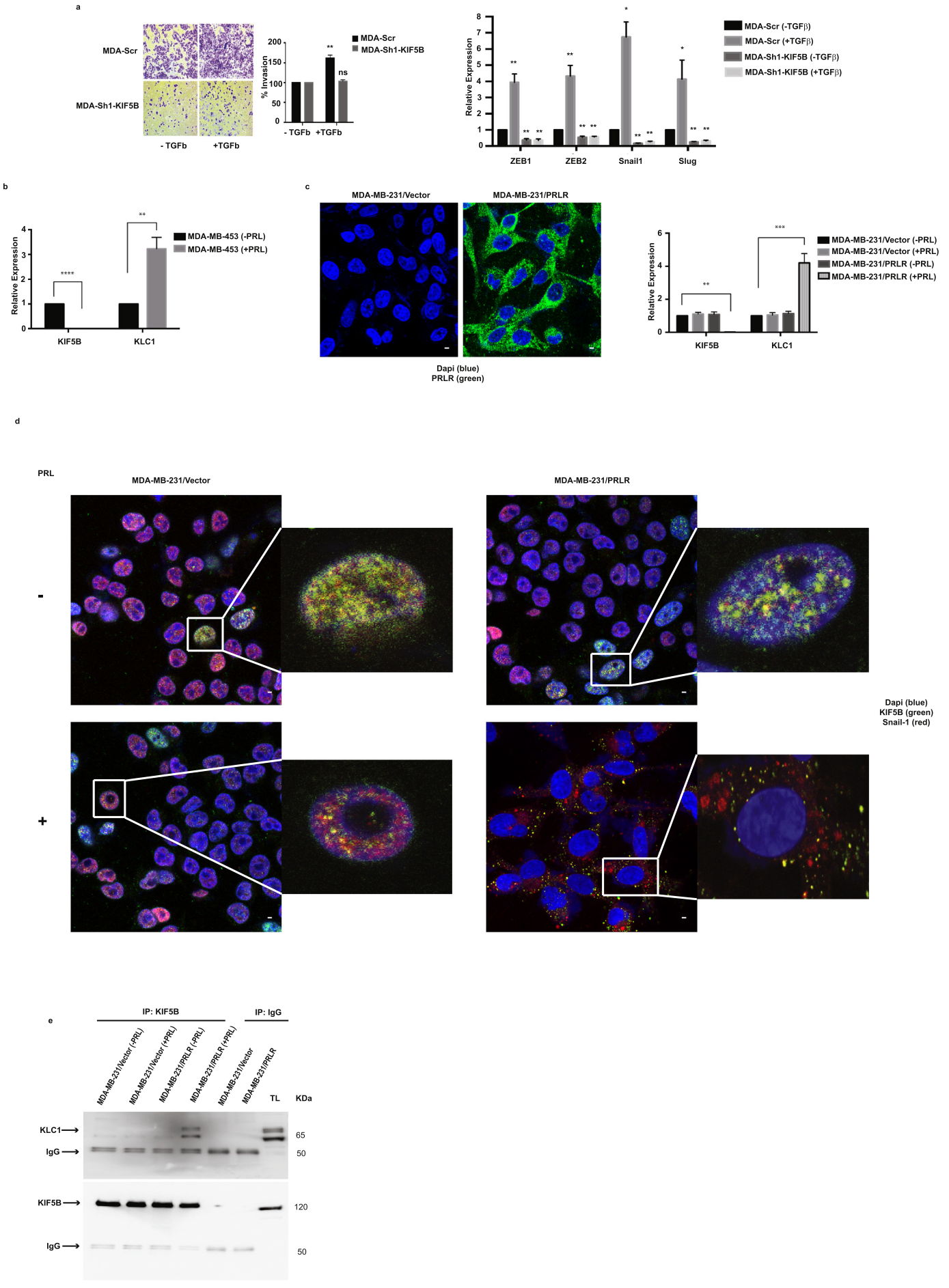
a
MDA-Scr
MDA-Sh1-KIF5B
- TGFb
+TGFb
% Invasion
MDA-Scr
MDA-Sh1-KIF5B
ns
Relative Expression
MDA-Scr (-TGFβ)
MDA-Scr (+TGFβ)
MDA-Sh1-KIF5B (-TGFβ)
MDA-Sh1-KIF5B (+TGFβ)
ZEB1
ZEB2
Snail1
Slug
b
Relative Expression
MDA-MB-453 (-PRL)
MDA-MB-453 (+PRL)
KIF5B
KLC1
c
MDA-MB-231/Vector
MDA-MB-231/PRLR
Dapi (blue)
PRLR (green)
Relative Expression
MDA-MB-231/Vector (-PRL)
MDA-MB-231/Vector (+PRL)
MDA-MB-231/PRLR (-PRL)
MDA-MB-231/PRLR (+PRL)
KIF5B
KLC1
d
PRL
MDA-MB-231/Vector
MDA-MB-231/PRLR
-
+
Dapi (blue)
KIF5B (green)
Snail-1 (red)
e
IP: KIF5B
IP: IgG
MDA-MB-231/Vector (-PRL)
MDA-MB-231/Vector (+PRL)
MDA-MB-231/PRLR (-PRL)
MDA-MB-231/PRLR (+PRL)
MDA-MB-231/Vector
MDA-MB-231/PRLR
TL
KDa
KLC1
IgG
KIF5B
IgG
65
50
120
50

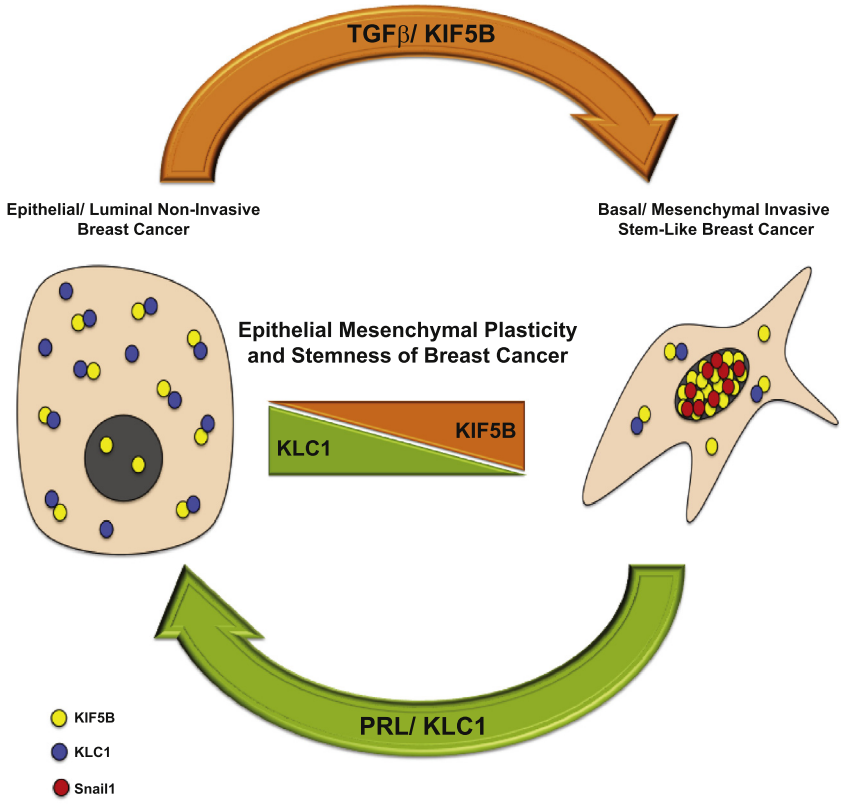

Fig. 8. KIF5B/KLC1 complex regulates epithelial mesenchymal plasticity programing in breast cancer determining breast cancer phenotype, stemness and aggressiveness. Expression levels of KIF5B and KLC1 varies according to the molecular subtypes of breast cancer. Whereas KLC1 is expressed in the luminal/epithelial subtypes, KIF5B is expressed in the mesenchymal basal subtype showing novel nuclear accumulation and interaction with Snail1 transcription factor. Moreover, KIF5B/KLC1 dynamic plays a central role in TGFβ and PRL regulation of EMP in breast cancer.

differentiated, grade II (60.38%) and grade I (31.58%) tumors ($P = .01$) (Fig. 6B, right panel). This data implicates KIF5B as a novel clinically relevant biomarker of high-grade invasive breast cancer.

2.7. KIF5B/KLC1 function downstream of TGF-β and PRL in TN-basal-like/claudin low cells

Our results so far emphasized a key role for kinesin-1 components KIF5B/KLC1 in regulating EMP in breast cancer. Extensive research has identified the growth factor TGFβ as a critical inducer of EMT, stemness, invasion and tumorigenesis in TN-basal-like/claudin low cells. Whereas, we have previously shown PRL to block TGF β function and to suppress EMT, invasion and tumorigenesis of TN-basal-like/claudin low cells [40–42]. Therefore, next we examined whether KIF5B regulates TGFβ-mediated pro-invasive function. Interestingly, we found that loss of KIF5B expression in MDA-MB-231 cells significantly blocked TGFβ-mediated cell invasion (Fig. 7A, left panel). To further study the role of KIF5B in mediating TGFβ regulation of EMT, we examined TGFβ induced expression of several EMT markers including ZEB1, ZEB2, Snail1 and Slug in MDA-Scr and MDA-Sh1-KIF5B cells. Interestingly, we found that loss of KIF5B abrogated TGFβ induced EMT markers expression implicating KIF5B in TGFβ induced EMT and cellular invasion capacity (Fig. 7A, right panel). To further study the role of TGFβ in regulating KIF5B expression, we next assessed the expression of KIF5B following TGFβ treatment of MDA-MB-231 cells. Our data did not show a significant change in KIF5B expression following TGFβ treatment (Supplementary Fig. S4B). Next, we investigated PRL regulation of KIF5B/KLC1 function. Interestingly, as seen in Fig. 7B, PRL treatment of MDA-MB-453 cells, TN-LAR subgroup has been shown previously to express PRLR endogenously [8], resulted in a significant suppression of KIF5B m-RNA levels concomitant with a significant increase in KLC1 m-RNA expression levels. These results were further confirmed using the TN-basal-like/claudin low cell line MDA-MB-231 cells engineered to overexpress the PRLR upon doxycycline treatment, designated as MDA-MB-231/PRLR cells [8]. The ectopic expression of PRLR in MDA-MB-231/PRLR cells was confirmed using IF analyses (Fig. 7C, left panel). As can be seen in Fig. 7C, right panel, upon doxycycline treatment, whereas PRL treatment suppressed KIFB expression, it resulted in increased expression of KLC1. We then evaluated the role of PRL in regulating KIF5B and Snail-1 nuclear accumulation, using the MDA-MB-231/PRLR cell model system. As shown in Fig. 7D, our data show that PRL treatment of MDA-MB-231/PRLR cells induced to express the

Fig. 7. KIF5B/KLC1 loop downstream of TGFβ and PRL in TNBC. A. Left panel, quantitative invasion assays of MDA-MB-231-Scr and MDA-MB-231-Sh1-KIF5B following TGFβ stimulation. Results presented are of triplicates of three independent experiments $^{***}p \le .001$ (Student's *t*-test). Right panel, m-RNA levels of EMT transcription factors ZEB1, ZEB2, Snail1 and Slug using q-RT-PCR in MDA-MB-231-Scr and MDA-MB-231-Sh1-KIF5B following TGFβ stimulation. Results are expressed as relative expression of triplicates of three independent experiments $^{**}p \le .01$, $^{*}p \le .05$ (one-way ANOVA). B. MDA-MB-453 cells were treated with rhPRL (150 ng/ml) for 24 h and the expression of KIF5B and KLC1 mRNA were examined using q-RT-PCR. Results are expressed as relative expression of triplicates of three independent experiments $^{****}p \le .0001$ and $^{**}p \le .01$ (Student's *t*-test). C. Left panel, confocal immunofluorescence images of PRLR (green) and nucleus (Dapi) (blue) of control MDA-MB-231/Vector and MDA-MB-231/PRLR. Right panel, control MDA-MB-231/Vector and MDA-MB-231/PRLR cells were treated or not with dox (100 ng/ml) and rhPRL (250 ng/ml) for 24 h. KIF5B and KLC1 mRNA expression were assessed using q-RT-PCR (one-way ANOVA). D. Confocal immunofluorescence images of KIF5B (green), Snail1 (red) and nucleus (Dapi) (blue) of MDA-MB-231/Vector and MDA-MB-231/PRLR cells following treatment or not with rhPRL (250 ng/ml) for 72 h. Scale bar, 10 μm. E. MDA-MB-231/Vector and MDA-MB-231/PRLR treated or not with rhPRL for 72 h were lysed and immunoprecipitations were performed using a rabbit monoclonal antibody against KIF5B or control normal rabbit IgG. Western blotting was carried out using a rabbit monoclonal antibody against KLC1. TL: total lysates.

PRLR, resulted in the re-localization of both KIF5B and Snail-1 to the cytoplasm, while no change in relocalization of the two proteins was observed in control cells. Finally, we also found that PRL treatment of MDA-MB-231/PRLR cells promotes the physical interaction between KIF5B and KLC1 (Fig. 7E). Together, these results emphasize a role for KIF5B/KLC1 in TGFβ and PRL regulation of EMP, highlighting a central role for KIF5B in mediating TGFβ pro-invasive activities and establishing the ability of PRL to regulate and suppress KIF5B function in TN-basal-like/claudin low cells.

3. Discussion

Kinesins encompass a large family of proteins that are well-known to mediate intracellular movement and cytoplasmic transport of membranous organelles and macromolecules along the microtubules network. Kinesin-driven transport is mediated by the concert function of two subunits forming a complex of the motor protein (KHC) and the adaptor protein (KLC) [10,11]. Here we present evidence highlighting for the first time that kinesin-1 subunits, KIF5B and KLC1, as distinct regulators of EMP thereby contributing to breast cancer heterogeneity and aggressiveness (Fig. 8).

3.1. The differential expression of KIF5B vs KLC1 in breast Cancer

The roles of Kinesin-1subunits KIF5B and KLC1 in breast tumorigenesis are still to be fully determined. Here using IHC analysis of breast cancer clinical cases we found KIF5B to be highly expressed in invasive ductal carcinoma and to be associated with poorly differentiated tumors. Moreover, and in agreement with a previous report [20], our IHC data also showed that TNBC clinical cases to exhibit high expression levels of KIF5B in comparison to other breast cancer subtypes. This finding was further confirmed using large bioinformatics dataset showing KIF5B to be enriched in the basal subtype based on PAM50 and Hu et al., subclassifications. These results together implicate KIF5B as a novel biomarker of high-grade invasive breast cancer. To further examine the expression of KIF5B in relation to breast cancer subtypes, we made use of breast cancer cell lines representative of the various breast cancer molecular subtypes [24–26]. Importantly, our data showed that KIF5B to be overexpressed in breast cancer cell lines characterized as TN-basal-like/claudin low subtype and least expressed in cell lines representative of the luminal/epithelial subtype. Importantly, cell fractionation experiments showed enrichment of KIF5B within the nuclear compartment of only TN-basal-like/claudin low cells. On the other hand, expression of KLC1, was found to correlate with favorable patient outcome and was found to exhibit different expression pattern than KIF5B. Interestingly, breast cancer cell lines as well as bioinformatics data of clinical breast cancer cases, showed KLC1 to be most expressed in luminal breast cancer subtypes including luminal A, luminal B and Her2-E and least expressed in basal-like subtype. Off note, no nuclear accumulation of KLC1 was observed in all breast cancer cells examined. Together our data emphasizes the differential expression and highlight possible independent functions of these two proteins in breast cancer.

3.2. Role of Kinesin-1 subunits (KIF5B/KLC1) in determining EMP

EMP is believed to be a critical regulator of cancer heterogeneity, disease progression and metastasis. When fully implemented cancer cells will acquire stem-like mesenchymal features exhibiting invasive/metastatic behavior resulting in high grade malignancy and resistance to available therapies. EMP may also contribute to molecular subtype conversion. Indeed, it has been shown that metastatic breast tumors of luminal but not basal-like subtype may undergo interconversion to more aggressive subtype [43]. These considerations underscore the interest in identifying further markers and molecular players driving the transition and switch from epithelial to mesenchymal states providing closer insights into understanding breast cancer progression and opening new avenues to more advanced therapies. TN-basal-like/claudin low breast cancer cells are known to be enriched for genes associated with EMT and to exhibit full EMT [24,44]. Our data showed that loss of KIF5B expression in these basal-like/claudin low breast cancer cells resulted in suppression of cell viability, EMT, migration, invasion, stemness and metastatic colonization of the lung. This result highlight KIF5B as a critical regulator of the EMP programming associated with the TN-basal-like/claudin low breast cancer subtype. On the other hand, KLC1 was found to be required to maintain an epithelial phenotype and to suppress EMT as well as stem cell markers endowing the cells with less invasive and less aggressive features. How kinesin1 regulates EMP is still to be fully discovered and it may involve various mechanisms. A previous report did show KIF5B to contribute to cell migration as part of the formation of invadopodia within the cytoplasm in the context of NT-basal-like/claudin low breast cancer cells [20]. Importantly, our data point to a new mechanism through which KIF5B may contribute to EMP. Indeed, we found KIF5B to localize in the nucleus in NT-basal-like/claudin low breast cancer cells. Moreover, we found KIF5B to interact with the EMT inducer Snail1 transcription factor in these cells. Still, further IF analyses showed heterogenous nuclear co-localization of KIF5B and Snail1, suggesting that KIF5B may have additional nuclear functions independent of Snail1. Additionally, we found that loss of KIF5B in TN-basal-like/claudin low breast cancer cells led to the re-localization of Snail 1 to the cytoplasm suggesting that KIF5B may play a role in Snail1 nuclear localization in these cells. Interestingly, PRL was found to regulate both KIF5B and Snail1 nuclear localization. Indeed, following PRL treatment of TN-basal-like/claudin low breast cancer cells KIF5B and Snail1 were excluded from the nucleus and partially co-localized in the cytoplasm. Moreover, we found that loss of KLC1 to be a determinant in the nuclear accumulation of KIF5B. These data suggest that KIF5B/KLC1 determine the transition between epithelial and mesenchymal phenotypes thereby defining the EMP status and aggressiveness of breast cancer.

3.3. Regulation of the EMP inducer TGFβ and the EMP suppressor PRL of kinesin-1 subunits KIF5B/KLC1 in breast cancer

Extensive studies have placed TGFβ ligands “center-stage” in regulating EMP leading to breast cancer cell invasion, metastasis and stemness [45]. On the other hand, PRL is known to play an essential role in regulating mammary alveologenesis during pregnancy lactation cycle [45–47]. Recently, PRL was shown to have direct effects in inducing apical/basal polarity and mammary luminal/epithelial stem cell terminal differentiation [23]. Interestingly, PRL was also found to have negative cross-talk with TGFb-Smad pathway and to suppress EMT, invasion and the tumorigenic phenotype of TNBC cells highlighting PRL as a critical suppressor of EMP [7,8,42]. Interestingly, our data implicates a central role for KIF5B/KLC1 loop in TGFβ and PRL regulation of EMP in breast cancer. Whereas TGFβ-pro-invasive activity requires KIF5B, PRL blocks KIF5B function through stable KIF5B/KLC1 complex formation there by suppressing EMP.

This manuscript highlights the role of kinesin-1 subunits KIF5B/KLC1 in breast cancer. While kinesin-1 is a large superfamily compromising various protein members, further studies are needed to investigate the role of other KIFs and KLCs in relation to each other as well as their role in breast cancer. Collectively, our study revealed a new understanding of the role of kinesin-1 in breast cancer mediating EMP programing. We propose here that the expression pattern of the two components of kinesin-1, KIF5B and KLC1, play an important role in determining breast cancer phenotype and aggressiveness.

4. Material and methods

4.1. Antibodies, plasmids and reagents

Antibodies: anti-KIF5B rabbit monoclonal antibody (abcam #ab167429), anti-UKHC rabbit polyclonal antibody (Santa-Cruz

#sc-28538), anti-KLC1 rabbit monoclonal antibody (abcam #ab174273), anti-PRLR rabbit polyclonal antibody (Santa-Cruz #sc-20992), anti-SNAIL1 goat polyclonal antibody (Santa-Cruz #sc-10433), anti-Cytokeratin 18 mouse monoclonal antibody (Santa-Cruz #sc-32329), anti-E-Cadherin mouse monoclonal antibody (BD Biosciences #610182) and anti-CD44 mouse monoclonal antibody (BD Biosciences #555478).

Antibodies used for FACS analysis were FITC mouse anti-human CD24 (BD Biosciences #555427) and APC mouse anti-human CD44 (BD Biosciences #559942).

Secondary antibodies used were goat anti-rabbit IgG HRP (Santa-Cruz #sc-2004), rabbit anti-goat IgG-HRP (Santa-Cruz #sc-2922) as well as goat anti-mouse IgG-HRP (Santa-Cruz #sc-2005). Secondary antibodies for confocal immunofluorescence studies were: donkey anti-rabbit IgG (H+L) Fluor 546 (Invitrogen), donkey anti-mouse Fluor 488 (Invitrogen), donkey anti-goat IgG-R Rhodamine conjugated (Santa-Cruz #sc-2094) and Alexa Fluor 568 phalloidin (Invitrogen #A12380).

The dilutions of antibodies for western blotting analysis are as indicated: 1: 1000 for all primary antibodies. The dilutions for secondary antibodies for western blotting analysis are 1:5000. For immunofluorescence staining: 1:100 for primary antibodies and 1: 200 for secondary antibodies. The dilution for antibodies for FACS analysis is 20:100 as recommended.

Other reagents used include: Recombinant human prolactin (rhPRL) (150 ng/ml and 250 ng/ml) used for human cell stimulation was purchased from Feldan Therapeutics (1F-02-008), Recombinant ovine prolactin (oPRL) (2 μg/ml) used for HC11 cell stimulation was purchased from Sigma-Aldrich (L6520-SIGMA), SosoFast EvaGreen Supermix (Bio-Rad # 172-5201), protein A-Sepharose beads (Amersham Biosciences and GE Healthcare), 12-well plates HTS multi-well insert system format (BD Falcon) and 96-well plates (Corning #3753 and Fisher #7201216).

4.2. Cell culture

Normal mammary epithelial cells: mouse HC11 cells were obtained from N. Hynes (Friedrich Miescher Institute, Basel, Switzerland) and were maintained in RPMI–1640 containing 10% fetal bovine serum (FBS) (Multicell Invitrogen). Human breast cancer cells: MDA-MB-231 obtained from Dr. Shafaat Rabbani (McGill University), MDA-MB-453, SKBR3 and BT474 were obtained from Dr. Morag Park (McGill University), SCP2 and SUM159 were obtained from Dr. Jean Jacques Lebrun (McGill University). MDA-MB-231, MDA-MB-453, SKBR3 MCF7 and SCP2 cells were maintained in DMEM media (Multicell Invitrogen) containing 10% fetal bovine serum (FBS) (Multicell Invitrogen). SUM159 were maintained in Ham F-12 media (Gibco by Life Technologies) containing 5% fetal bovine serum (FBS) (Multicell Invitrogen).

4.3. KIF5B stable knock-down in human breast cancer cells

Lentiviral particles expressing human shRNA against KIF5B was obtained from Sigma and scramble shRNA were obtained from Addgene. The scramble shRNA is in pLKO.1 (Addgene plasmid 338651) and human KIF5B MISSION shRNA in bacterial GlycerolStock (TRCN#0000338651).

(CCGGTCGGCAACTTTAGCGAGTATACTCGAGTATACTCGCTAAAGT TGCCGATTTTTG) and (TRCN#0000338580)

(CCGGTTACAACTGTGGCCCTATTTACTCGAGTAAATAGGGCCACAG TTGTAATTTTTG). MDA-MB-231, SUM159 and T47D cells were infected with lentiviral particles. Stable cell lines were then generated using puromycin selection (InvivoGen) 1 μg/ml puromycin for MDA-MB-231 and 2 μg/ml for SU159 and T47D cells.

4.4. KLC1 transient knock-down in human breast cancer cells

Silencer pre designed SiRNA against human KLC1 and Negative control SiRNA were obtained from Thermo Fisher Scientific AM51331 and AM16708. T47D and SKBR3 cells were infected with 28 nM SiRNA using lipofectamine 2000 protocol obtained from Thermo Fisher Scientific.

4.5. Snail1 transient knock-down in human breast cancer cells

Silencer pre designed SiRNA against human Snail1 and Negative control SiRNA were obtained from Thermo Fisher Scientific AM16708. MDA-MB-231 cells were infected with 28 nM SiRNA using lipofectamine 2000 protocol obtained from Thermo Fisher Scientific.

4.6. Western blotting analysis

Nuclear extraction lysates were collected by hypotonic buffer (10 mM HEPES-KOH pH 7.9, 1.5 mM $MgCl_2$, 10 mM KCl, 0.5 mM DDT, 1 mM Na_3VO_4, 20 mM NaF and Protease inhibitors cocktail). Then, the pellet was washed with 1× PBS 3 times. After wash, High salt buffer (20 mM HEPES-KOH pH 7.9,25% glycerol, 420 mM NaCl, 1.5 mM $MgCl_2$, 0.2 mM EDTA pH 8.0, 1 mM Na_3VO_4, 20 mM NaF and Protease inhibitors cocktail) were used to get the nuclear extract from the pellet. 20 μg protein was loaded in the SDS-PAGE gel.

Total protein lysates were obtained using RIPA lysis buffer (50 mM Tris pH 8, 150 mM sodium chloride, 1% NP-40, 0.5% sodium deoxycholate, 0.1% SDS, 1 mM Na_3VO_4 and Protease inhibitors cocktail). 30 μg proteins were loaded in the gel. Cell lysates were separated by electrophoresis in 8–12% sodiumdodecyl sulphate-polyacrylamide gradient minigel (SDS-PAGE) and electrophoretically transferred to anitrocellulose membrane. Western blots were probed with the relevant primary antibodies and secondary antibodies.

4.7. Immunoprecipitation

RIPA lysis buffer (50 mM Tris pH 8, 150 mM sodium chloride, 1% NP-40, 0.5% sodium deoxycholate, 0.1% SDS, 1 mM Na3VO4 and Protease inhibitors cocktail) was used to obtain the total protein lysates. Mixer of 1 μg of anti-KIF5B antibody, protein A/G beads (20 μl) and 500 μg of cell lysates were incubated for 3 h at 4 °C. After washing the beads, western blotting with SDS-PAGE gel was performed with specific antibodies.

4.8. Immunofluorescence

Cells were grown on coverslips with 80% confluency. Fixation process were performed of coverslips coated with cells in 4% Paraformaldehyde for 15 min at room temperature, followed by permeabilization process with 0.1% Triton X-100 (Fisher). Cells were subsequently immunostained with primary antibody for an overnight period at 4 °C and followed by secondary antibody and Dapi for 1 h at room temperature. Mounting media (Lerner # 13800) was used to mount the coverslips and stored at 4 °C. Confocal microscopy was performed using Zeiss LSM 780 confocal microscope equipped with a Plan- Apochromat x63-1.4 oil immersion objective.

4.9. RNA isolation and RT-qPCR

HC11 cells were grown to confluence then allowed to undergo differentiation for 24 h in media containing 10% FBS, insulin and hydrocortisone. Then, cells were starved or treated with ovine PRL (sigma) for 24 h. Breast cancer cells T47D, MCF7, BT474, SKBR3, MDA-MB-453, MDA-MB-231, SCP2 and SUM159 were also grown to confluence before RNA extraction was performed. MDA-MB-453 cells, MDA-MB-231/Vector and MDA-MB-231/PRLR were grown to confluence then were starved or treated with recombinant human PRL for 48 h. All cells

were lysed in 1 ml of trizol. Total RNA was isolated following RNA extraction protocol (Abcam, United States).

Nanodrop was used to quantify RNA concentrations at 260 nm. Total RNA 1 μg was used for reverse transcription by using (iScript Reverse Transcription supermix kit # 170-8841). RT-qPCR of KIF5B, Slug, Snail, Twist, FN1, Vimentin, ZEB1, ZEB2, PRLR E-cadherin, CK18, CD44, CD24, OCT4, NANOG and SOX2) was performed.

4.10. MTT assay

5.103 cells were seeded into 96-well plate and grown for a period 2 to 8 days. Then, cells were incubated with 3-(4,5-dimethyl-2-thiazolyl)-2,5-diphenyl-2H-tetrazolium bromide (MTT) at 37 °C for 2 h.

4.11. Scratch assay

5×10^3 cells were seeded on 6 well plate and grown until reached confluency. A straight scratch was obtained by yellow pipette tip and scratch or wound was monitoring by taking picture at 0, 24 and 48 h.

4.12. Invasion assay

80×10^3 cells were seeded in 24-well plates HTS multi-well insert system coated with Matrigel. Invasion assays were performed for 24 h migrated cells were counted using five fields of triplicates for each experimental point.

4.13. Soft agar transformation assay

30×10^3 cells were seeded into 24-well plate coated with 1% agar gel and grown in growth media with 0.6% agar for 3 weeks. Colonies were stained by 0.05% crystal blue. Number of colonies was counted using low power lens microscopy.

4.14. Tumorsphere assay

MDA-Scr and MDA-Sh-KIF5B cells were seeded in ultra low-attachment 24-well plate (Corning), and cultured in serum-free DMEM medium supplemented with 10 ng/ml EGF, 10 ng/ml bFGF and 1 × B27 (Invitrogen). The plate was incubated at 37 °C with 5% CO_2 for 7 days, without moving the plate. Tumorspheres were counted using ImageJ software.

4.15. Gene expression analysis

Publically available (ONCOMINE) and (GOBO) databases were used to determine associations between KIF5B and KLC1 m-RNA expression levels and different clinicopathological parameters in large human breast cancer cohorts. KM plotter was used to determine associations of gene expression in relation to patient outcome.

4.16. Tissue microarray

TMA of 102 cases was commercially purchased from Pantomics (Richmond, CA; BRC1021). TMA include information containing; age, grade, stage and TNM. The virtual H & E slides for those cases were available and were reviewed by a pathologist to confirm the diagnosis and that they are representative of the tumor.

4.17. Immunohistochemistry

Immunohistochemical staining was performed to paraffin embedded slides. After deparaffinization and rehydration slides were immersed in retrieval solution (sodium citrate 10 mM, pH 6.0 buffer). The slides were incubated in hydrogen peroxide block s, followed by Ultra V Block. Slides were incubated with a rabbit anti-KIF5B Antibody. UltraVision LP Detection System HRP Polymer & DAP Plus Chromogen (Thermo Fisher Scientific, Fremont CA) was used for detection. The TMA slides were scanned using Aperio XT slide scanner (Leica Biosystems).

4.18. Immunohistochemistry scoring

Quantitative IHC scoring systems were used to evaluate KIF5B immunostaining. In brief, a representative pathologist-annotated malignant region was selected for each core using images of 40 × magnification from digital IHC-stained TMA slides. The mean positive pixel count (PPC) for each representative region was obtained using positive pixel count (PPC) algorithm (Aperio). The lower PPC count indicates higher IHC staining intensity. The staining intensity was divided equally into 4 categories. For KIF5B cases with PPC ≥ 95 considered +3, 96–110 PPC considered +2, 111–127 considered +1 and cases with PPC ≤ 128 considered as score 0. ER, PR, HER-2 and Ki67 classification into molecular subtypes was done as previously described [48].

4.19. Animal models

All experimental animal work was performed in a specific-pathogen-free animal facility according to the guidelines and ethical regulations of the Research Institute McGill University Health Centre approved animal used protocol (#2014-7492) in accordance with Canadian Council of animal care guidelines.

4.20. KIF5B mammary fat pad NSG mouse xenografts

14 Female NSG mice were purchased from Charles River Laboratories (Sain-Constant, QC, Canada), housed and maintained under specific pathogen-free conditions (RI-MUHC animal facility). The mice were randomly divided into two groups ($n = 7$ mice per group). At 7 to 9 weeks of age, the first group was injected in the fourth-left mammary fat pad with 1×10^6 MDA-MB-231-Scr and the second group was injected with MDA-MB-231-Sh-KIF5B. Tumor growth were monitored up to 7 weeks after injection. When tumors were detectable, tumor size was measured with a vernier caliper (Mitutoyo, Kawasaki, Japan) and calculated using the formula [length + width2]/2. Mice were sacrificed by CO2 asphyxiation.

4.21. KIF5B tail vein NOD-SCID mouse xenografts

12 Female NOD-SCID mice were purchased from Charles River Laboratories (Sain-Constant, QC, Canada), housed and maintained under specific pathogen-free conditions (RI-MUHC animal facility). The mice were randomly divided into two groups ($n = 6$ mice per group). At 7 to 9 weeks of age, the first group was injected in the tail vein with 5×10^5 MDA-MB-231-Scr and the second group was injected with MDA-MB-231-Sh-KIF5B. Mice were monitored up to 5 weeks after injection. Mice were sacrificed by CO2 asphyxiation and lungs were collected.

4.22. KLC1 tail vein NSG mouse xenografts

12 Female NSG mice were purchased from Charles River Laboratories (Sain-Constant, QC, Canada), housed and maintained under specific pathogen-free conditions (RI-MUHC animal facility). The mice were randomly divided into two groups (n = 6 mice per group). At 7 to 9 weeks of age, the first group was injected in the tail vein with 5×10^5 T47D-Si-control and the second group was injected with T47D-Si-KLC1. Mice were monitored up to 5 weeks after injection. Mice were sacrificed by CO2 asphyxiation and lungs were collected.

4.23. Statistical analysis

Statistical analysis were performed using GraphPad prism 6 software using Student's *t*-test or one-way ANOVA analysis accordingly. Results were shown as mean ± SEM and $P < .05$ was considered as cut-off for significant association.

Supplementary data to this article can be found online at https://doi.org/10.1016/j.ebiom.2019.06.009.

Authors' contributions

AM: Designed, performed experiments and drafting the article. IH: Performed and analyzed IHC experiments, some bioinformatics data NB: Performed the nuclear extraction assay, immunoprecipitation assay and contributed to drafting the article NW: Performed *in vivo* experiments JJL: Contributed design and revising the article, SA: Principal research design and supervision of the project and drafting of the article.

Conflicts of interest

The authors declare no conflicts of interest.

Data deposition and materials sharing

https://www.pantomics.com/tissue-arrays/reproductive-system/breast/brc1021

Acknowledgements

We would like to thank the confocal Imaging Platform of the Research Institute, McGill University Health Centre. The authors declare no competing financial interests.

J.J. Lebrun is the recipient of the McGill Sir William Dawson Research Chair. This work was supported by the Canadian Institutes of Health Research (operating grants #233437 and 233438) granted to Suhad Ali. The funders had no role in study design, data collection, data analysis, interpretation, writing of the report.

References

[1] Skibinski A, Kuperwasser C. The origin of breast tumor heterogeneity. Oncogene 2015;34:5309–16.
[2] Chaffer CL, San Juan BP, Lim E, Weinberg RA. EMT, cell plasticity and metastasis. Cancer Metastasis Rev 2016;35:645–54.
[3] Viale G. The current state of breast cancer classification. Ann Oncol 2012;23(Suppl. 10):x207–10.
[4] Sorlie T, et al. Gene expression patterns of breast carcinomas distinguish tumor subclasses with clinical implications. Proc Natl Acad Sci U S A 2001;98:10869–74.
[5] Katsuno Y, Lamouille S, Derynck R. TGF-beta signaling and epithelial-mesenchymal transition in cancer progression. Curr Opin Oncol 2013;25:76–84.
[6] Massague J, Obenauf AC. Metastatic colonization by circulating tumour cells. Nature 2016;529:298–306.
[7] Nouhi Z, et al. Defining the role of prolactin as an invasion suppressor hormone in breast cancer cells. Cancer Res 2006;66:1824–32.
[8] Lopez-Ozuna VM, Hachim IY, Hachim MY, Lebrun JJ, Ali S. Prolactin pro-differentiation pathway in triple negative breast cancer: impact on prognosis and potential therapy. Sci Rep 2016;6:30934.
[9] Lawrence CJ, et al. A standardized kinesin nomenclature. J Cell Biol 2004;167:19–22.
[10] Hirokawa N, Noda Y, Tanaka Y, Niwa S. Kinesin superfamily motor proteins and intracellular transport. Nat Rev Mol Cell Biol 2009;10:682–96.
[11] Gindhart Jr JG, Desai CJ, Beushausen S, Zinn K, Goldstein LS. Kinesin light chains are essential for axonal transport in Drosophila. J Cell Biol 1998;141:443–54.
[12] Cyrus BF, Muller WA. A unique role for endothelial cell Kinesin light chain 1, variant 1 in leukocyte transendothelial migration. Am J Pathol 2016;186:1375–86.
[13] Verhey KJ, Hammond JW. Traffic control: regulation of kinesin motors. Nat Rev Mol Cell Biol 2009;10:765–77.
[14] Salinas S, Bilsland LG, Schiavo G. Molecular landmarks along the axonal route: axonal transport in health and disease. Curr Opin Cell Biol 2008;20:445–53.
[15] Verhey KJ, Kaul N, Soppina V. Kinesin assembly and movement in cells. Annu Rev Biophys 2011;40:267–88.
[16] Wang Z, et al. Kif5b controls the localization of myofibril components for their assembly and linkage to the myotendinous junctions. Development 2013;140:617–26.
[17] Wang Z, et al. Dissect Kif5b in nuclear positioning during myogenesis: the light chain binding domain and the autoinhibitory peptide are both indispensable. Biochem Biophys Res Commun 2013;432:242–7.
[18] Cui J, et al. Analysis of Kif5b expression during mouse kidney development. PloS one 2015;10:e0126002.
[19] Cardoso CM, et al. Depletion of kinesin 5B affects lysosomal distribution and stability and induces peri-nuclear accumulation of autophagosomes in cancer cells. PloS one 2009;4:e4424.
[20] Marchesin V, et al. ARF6-JIP3/4 regulate endosomal tubules for MT1-MMP exocytosis in cancer invasion. J Cell Biol 2015;211:339–58.
[21] Wang Z, et al. Binding of PLD2-generated phosphatidic acid to KIF5B promotes MT1-MMP surface trafficking and lung metastasis of mouse breast cancer cells. Dev Cell 2017;43:P186–P197.e7.
[22] Hachim IY, Shams A, Lebrun JJ, Ali S. A favorable role of prolactin in human breast cancer reveals novel pathway-based gene signatures indicative of tumor differentiation and favorable patient outcome. Hum Pathol 2016;53:142–52.
[23] Liu F, et al. Prolactin/Jak2 directs apical/basal polarization and luminal linage maturation of mammary epithelial cells through regulation of the Erk1/2 pathway. Stem Cell Res 2015;15:376–83.
[24] Prat A, et al. Phenotypic and molecular characterization of the claudin-low intrinsic subtype of breast cancer. Breast Cancer Res 2010;12:R68.
[25] Lehmann BD, et al. Identification of human triple-negative breast cancer subtypes and preclinical models for selection of targeted therapies. J Clin Invest 2011;121:2750–67.
[26] Jiang G, et al. Comprehensive comparison of molecular portraits between cell lines and tumors in breast cancer. BMC Genomics 2016;17(Suppl. 7):525.
[27] Rahman A, Kamal A, Roberts EA, Goldstein LS. Defective kinesin heavy chain behavior in mouse kinesin light chain mutants. J Cell Biol 1999;146:1277–88.
[28] Adio S, Reth J, Bathe F, Woehlke G. Review: regulation mechanisms of Kinesin-1. J Muscle Res Cell Motil 2006;27:153–60.
[29] Rhodes DR, et al. ONCOMINE: a cancer microarray database and integrated data-mining platform. Neoplasia 2004;6:1–6.
[30] Parker JS, et al. Supervised risk predictor of breast cancer based on intrinsic subtypes. J Clin Oncol 2009;27:1160–7.
[31] Ringner M, Fredlund E, Hakkinen J, Borg A, Staaf J. GOBO: gene expression-based outcome for breast cancer online. PLoS One 2011;6:e17911.
[32] Gyorffy B, et al. An online survival analysis tool to rapidly assess the effect of 22,277 genes on breast cancer prognosis using microarray data of 1,809 patients. Breast Cancer Res Treat 2010;123:725–31.
[33] Wu Y, Sarkissyan M, Vadgama JV. Epithelial-mesenchymal transition and breast cancer. J Clin Med 2016;5.
[34] Ye X, et al. Upholding a role for EMT in breast cancer metastasis. Nature 2017;547:E1–3.
[35] Jin J, Krishnamachary B, Mironchik Y, Kobayashi H, Bhujwalla ZM. Phototheranostics of CD44-positive cell populations in triple negative breast cancer. Sci Rep 2016;6(27871).
[36] Dontu G, Al-Hajj M, Abdallah WM, Clarke MF, Wicha MS. Stem cells in normal breast development and breast cancer. Cell Prolif 2003;36(Suppl. 1):59–72.
[37] Fillmore C, Kuperwasser C. Human breast cancer stem cell markers CD44 and CD24: enriching for cells with functional properties in mice or in man? Breast Cancer Res 2007;9(303).
[38] Nieto MA. The ins and outs of the epithelial to mesenchymal transition in health and disease. Annu Rev Cell Dev Biol 2011;27:347–76.
[39] Thiery JP, Acloque H, Huang RY, Nieto MA. Epithelial-mesenchymal transitions in development and disease. Cell 2009;139:871–90.
[40] Mani SA, et al. The epithelial-mesenchymal transition generates cells with properties of stem cells. Cell 2008;133:704–15.
[41] Kim S, Lee J, Jeon M, Nam SJ, Lee JE. Elevated TGF-beta1 and -beta2 expression accelerates the epithelial to mesenchymal transition in triple-negative breast cancer cells. Cytokine 2015;75:151–8.
[42] Haines E, et al. Tyrosine phosphorylation of Grb2: role in prolactin/epidermal growth factor cross talk in mammary epithelial cell growth and differentiation. Mol Cell Biol 2009;29:2505–20.
[43] Cejalvo JM, et al. Intrinsic subtypes and gene expression profiles in primary and metastatic breast cancer. Cancer Res 2017;77:2213–21.
[44] Dias K, et al. Claudin-low breast cancer; clinical & pathological characteristics. PloS one 2017;12:e0168669.
[45] Lv ZD, et al. Transforming growth factor-beta 1 enhances the invasiveness of breast cancer cells by inducing a Smad2-dependent epithelial-to-mesenchymal transition. Oncol Rep 2013;29:219–25.
[46] Wagner KU, et al. Impaired alveologenesis and maintenance of secretory mammary epithelial cells in Jak2 conditional knockout mice. Mol Cell Biol 2004;24:5510–20.
[47] Cui Y, et al. Inactivation of Stat5 in mouse mammary epithelium during pregnancy reveals distinct functions in cell proliferation, survival, and differentiation. Mol Cell Biol 2004;24:8037–47.
[48] Hachim IY, Hachim MY, Lopez VM, Lebrun JJ, Ali S. Prolactin receptor expression is an independent favorable prognostic marker in human breast cancer. Appl Immunohistochem Mol Morphol 2016;24:238–45.